

Highlights

FLORA: A deep learning approach to predict forest attributes from heterogeneous LiDAR data

Emilie Vautier, Clément Mallet, Cédric Vega

- LiDAR acquisition variability affects forest attributes predictions.
- Nationwide French LiDAR dataset enable large-scale heterogeneous analysis.
- Deep learning exploits LiDAR point clouds while preserving forest structure for forest attributes estimation.
- Season-specific trained models fail across different phenology.
- Multi-season training improves robustness and national-scale transferability.

FLORA: A deep learning approach to predict forest attributes from heterogeneous LiDAR data

Emilie Vautier^{a,b,*}, Clément Mallet^a, Cédric Vega^{b,c}

^a*Univ Gustave Eiffel, Géodata Paris, IGN, LASTIG, F-77454 Marne-la-Vallée, France*

^b*Univ Gustave Eiffel, Géodata Paris, IGN, LIF, F-54000, Nancy, France*

^c*Université de Lorraine, Géodata Paris, IGN, LIF, F-54000 Nancy, France*

Abstract

Forest attributes are essential for national-scale resource monitoring. Among auxiliary data supporting National Forest Inventory (NFI) estimates, airborne LiDAR metrics are among the most strongly correlated with forest attributes. However, producing operational wall-to-wall predictions remains challenging when LiDAR data are acquired under heterogeneous conditions. As national LiDAR programs expand across Europe, variability in flight constraints, sensors, seasons, and scan angles becomes a major obstacle to consistent forest attribute mapping. Existing models are often local and struggle to generalize beyond their calibration domain, especially at national scale over structurally diverse forests.

We present FLORA (Forest LiDAR Octree Regression with Auxiliary Data), a deep learning framework predicting six forest attributes: dominant height, total volume, deciduous and coniferous volumes, basal area, and stem density, from heterogeneous LiDAR point clouds. FLORA combines an octree-based high-resolution backbone with ecological and spatiotemporal auxiliary variables through a late-fusion gating mechanism, enabling partial interpretability of contextual data contributions for each forest attribute prediction. Models are trained and evaluated using 32,052 National Forest Inventory plots across mainland France, using data from the French LiDAR HD program covering diverse forest types and acquisition conditions.

Experiments show that a single model trained jointly on leaf-on and leaf-off acquisitions outperforms season-specific models and improves cross-season robustness. Auxiliary variables provide modest overall gains but re-

*Corresponding author: Emilie Vautier. Email: emilie.vautier1@gmail.com

veal attribute-dependent contributions, particularly for species-specific volume prediction. The model achieves strong performance for dominant height (rRMSE \approx 12.3%, $R^2 \approx$ 0.88) and competitive results for total volume (rRMSE \approx 39%, $R^2 \approx$ 0.74). These results establish FLORA as a robust baseline for large-scale forest attribute estimation from national LiDAR programs.

Keywords: Airborne LiDAR, Deep learning, National forest inventory, Data heterogeneity, National scale

1. Introduction

National Forest Inventories (NFIs) are designed to estimate and sometimes to monitor the change in forests characteristics at National scale with a given level of reliability. In order to downscale NFI estimates without increasing the cost of field surveys while preserving the reliability of the estimates, methods have been developed to combine NFI data with auxiliary data. Those so-called Multisource Forest Inventories (MSNFIs) usually rely on remote sensing data selected for their correlation with the forest attributes of interest, their low cost, and their availability at the national scale, together with their regular long-term renewal (Tomppo et al., 2008). In terms of correlation, 3D data derived from airborne laser scanning, stereophotogrammetry, and, to a lesser extent, radar interferometry are the most suitable sources of auxiliary information for structural forest attributes such as volume and biomass (Borsah et al., 2023). With the development of national-scale LiDAR databases, interest in their use within MSNFIs has been renewed. That said, data acquisition and processing are not standardized, making their integration into MSNFIs a challenge.

LiDAR data processing methods are established for point clouds acquired locally, and often with similar acquisition conditions. Nevertheless, a significant challenge arises with national acquisitions, which often rely on point clouds acquired under varying acquisition conditions (Petras et al., 2023). Early studies have pointed out that LiDAR acquisition parameters such as flying altitude, scan angle, pulse density, and sensor characteristics influence the estimation of forest structural attributes. Næsset (2009) showed, from four Airborne Laser Scanning (ALS) acquisitions over 40 field plots in mature conifer forest, that instrument type, flying altitude, and pulse repetition frequency all affect ALS-derived height and density metrics, with systematic

differences between acquisitions of up to 2.5% for mean tree height and 10.7% for timber volume, despite only minor differences in overall model precision. Gopalakrishnan et al. (2015) further demonstrated, using linear regression on $\sim 1,800$ field plots across 76 heterogeneous ALS projects in the South-eastern US, that combining heterogeneous LiDAR datasets over large areas introduces additional variability, with factors such as point density, scan angle, and vegetation heterogeneity influencing model accuracy, though canopy height could still be predicted with a root mean squared error (RMSE) of 3.0 m ($R^2 = 0.74$), reduced to 2.4 m in structurally homogeneous stands. Qin et al. (2017) specifically highlighted the scan angle as a critical parameter for foliage profile retrieval, identifying an optimal angle of 20° regardless of flying altitude or pulse density, while showing that combining multiple scan angles can further improve estimation accuracy.

Differences between leaf-on and leaf-off acquisition conditions have been shown to substantially affect canopy structure representation and the estimation of forest attributes. In *deciduous* stands in particular, the absence of foliage leads to a greater penetration of the signal through the canopy, resulting in a higher number of single and last returns originating from the ground and a shift of the return distribution toward lower heights under leaf-off conditions (Ørka et al., 2010). These structural differences have direct consequences for model transferability: applying a k-nearest neighbors (kNN) algorithm, a non-parametric method that predicts values based on the most similar observations, to predict volume-related values by analyzing the volumes of the most similar data points, trained under leaf-on conditions to leaf-off data (and vice versa) introduces substantial bias and should therefore be avoided (Villikka et al., 2012). This degradation in performance has been quantified in boreal forest contexts using Random Forest models across two inventory areas in Finland, where cross-using leaf-on and leaf-off models increased relative Root Mean Square Error (rRMSE) and led to both over and underestimation, particularly in *deciduous*-dominated plots. In these cases, error nearly doubled (from $\sim 33\%$ to $\sim 56\%$) and bias reached up to 29%, although calibration via an empirical ratio estimator was shown to partially mitigate these errors (Maltamo et al., 2025). Consistent with these findings, further evidence shows that cross-application of random forest models and acquisition conditions results in large increases in error for both forest types, with average absolute increases of rRMSE up to 16.8% for coniferous stands and 25.8% for deciduous stands, reinforcing that such mismatches should be avoided (White et al., 2015). These results highlight the critical

importance of accounting for phenological conditions when developing and applying LiDAR-based forest attribute models.

The reliability of estimates also vary with the forest type (even at a coarse level such as *coniferous*, *deciduous*, and *mixed forests*). For *deciduous* trees, leaf conditions influence the distribution of points, with skewed distributions toward the upper crown in leaf-on conditions with limited penetration to the ground, to shifted point distribution toward lower canopy levels with increased ground sampling in leaf-off conditions (Davison et al., 2020). Pure *coniferous* stands tend to be minimally impacted by acquisition conditions (Wasser et al., 2013), albeit the residual presence of broadleaf trees, lower vegetation and partial winter needle thinning (Davison et al., 2020) still introduces variability. One can conclude that most recent findings and models are heavily area- and acquisition-dependent (Fareed et al., 2026).

Taken together, these acquisition-related and phenological sources of variability make it particularly challenging to develop forest variable estimation models that generalize beyond their local or regional scales, and the conditions under which they were trained. This motivates the development of more robust, large-scale approaches.

Estimating forest attributes at national scale with a single, generic model capable of handling a large diversity of forest types and LiDAR acquisition settings remains, to the best of our knowledge, an open problem as to date, the authors are not aware of such investigations. In this paper, we address this challenge by leveraging the French national LiDAR HD program. Such acquisition program provides a uniquely large and heterogeneous dataset of 3D point clouds, with minimum density of 10 pts/m² and acquisitions distributed across both leaf-off and leaf-on conditions. French forests are dominated at 68% by *deciduous* stands, a forest type whose structural signal is strongly modulated by phenology: such dataset captures a variability rarely encountered in previous studies. This heterogeneity is further compounded by the five-year acquisition window, which spans multiple campaigns conducted under different seasonal and instrumental conditions, making the dataset not only large but intrinsically variable.

Harmonization remains, to our knowledge, largely unexplored in this context, although several strategies have been proposed in the literature to address acquisition heterogeneity. One approach consists in developing separate estimation models for each acquisition campaign or season, as implemented

by Nilsson et al. (2017) within the Swedish NFI framework: block-specific (usually 25 km by 50 km in size) linear regression models were fitted using the nearest NFI plots to account for the variability introduced by different ALS sensors and acquisition settings across the country. Alternatively, linear mixed-effects models have been proposed to account for both forest type and acquisition variability, as demonstrated by Hauglin et al. (2021) in the context of the Norwegian forest resource map, where data from 367 ALS projects acquired over ten years were combined with NFI plots through stratification by species and maturity class. Species-specific models yielded rRMSE of 35%, 34%, 31% and 12% for volume, aboveground biomass, basal area and Lorey’s height, respectively, outperforming general unstratified models by 2–7 percentage points.

However, explicitly stratifying models by acquisition condition and forest type remains challenging at national scale, where the compounding diversity of forest composition, climate, and topography, combined with the difficulty of aggregating small areas due to error propagation (Walshe et al., 2021; Saarela et al., 2016; Breidenbach et al., 2014) limits the practical applicability of such approaches. The question of spatial transferability further illustrates these limitations: Soininen et al. (2025) proposed a Random Forest approach combining ALS and NFI data across Finland, yet reported a systematic increase in RMSE with geographic distance from the training set, highlighting the limited generalization capacity of such models under spatial heterogeneity. Moreover, phenology represents only one dimension of the problem: flight altitude, sensor type, and point density each influence point cloud properties in ways that interact with forest type and structure. This renders exhaustive stratification both impractical and potentially inadequate. A more robust solution requires a form of *harmonization*, whether applied at the input data level (making 3D point clouds similar in terms of geometry) or at the prediction level (estimating consistent forest variable whatever the above-mentioned fluctuations).

One straightforward approach would consist in homogenizing datasets by converting all 3D point clouds into a specific targeted condition (*e.g.*, leaf-on). However, beyond phenology, many other acquisition characteristics like flight altitude, sensor type, density as well as their interaction with each forest type and structure have been shown to affect point cloud properties (Jakubowski et al., 2013; LaRue et al., 2022). Explicitly normalizing for every known effect is a complex reconstruction task, and likely impractical for large-scale operational use on heterogeneous datasets (Rüetschi et al.,

2021). It is also based on the assumption that it is possible to retrieve the correct geometry of forests. However, the literature mainly focuses on point cloud completion and has only been addressed at the individual tree level or for opaque surfaces (Bornand et al., 2024; Luo et al., 2026).

Instead, another approach could focus on predicting similar outputs. It assumes a statistical model can capture such heterogeneity and can automatically learn to adjust its prediction to the acquisition and seasonal context. This hypothesis is supported by White et al. (2015). They showed, using Random Forest models trained on 787 ground plots in a lodgepole pine-dominated forest in Alberta, Canada, that pooling leaf-on and leaf-off data into a single model results in only marginal performance loss (<2% rRMSE for coniferous, near-zero for deciduous stands). This suggests that a single model can implicitly accommodate both acquisition conditions without explicit stratification. At larger scales, Hauglin et al. (2021) further demonstrated that such an approach remains feasible even under strong acquisition heterogeneity, successfully combining data from 367 ALS projects acquired over a decade across 17 Mha of Norwegian forest within a single modeling framework.

Traditional machine learning approaches rely on pairing carefully designed statistical features derived from point clouds with ground-truth measurements from forest inventory plots to perform predictions. Regression models for forest attributes (volume, biomass, basal area, etc.), typically based on Random forest and kNN algorithms, often struggle to generalize when applied over heterogeneous conditions. Even if methods like kNN have the advantage of providing confidence intervals using empirical quantiles of the neighbors or bootstrapping (Sagar et al., 2025), they are still limited by their ability to learn robust transferable representation (Villikka et al., 2012; Parra et al., 2025). Recent advances in deep learning (DL) offer new perspectives to overcome these limitations. Oehmcke et al. (2023) highlight that DL regression of forest attributes can produce more accurate results compared to state-of-the-art machine learning methods. By operating directly on raw point clouds, DL models preserve the full three-dimensional structure of the data and automatically learn relevant spatial features, bypassing the need for manual feature selection, and fluctuation in the local geometry of point clouds.

Several DL architectures have been proposed to process 3D point clouds, broadly falling into two categories: point-based and voxel-based approaches.

Point-based approaches rely on sampling or grouping strategies to capture local context (Wu et al., 2024; Geist et al., 2025), a strategy that is not well suited to the structural irregularity of forest canopies, where vegetation density varies continuously and no clear object boundaries exist. Voxel-based discretizations, in contrast, preserve structural information while maintaining computational efficiency, and are better adapted to the sparse and heterogeneous nature of forest point clouds.

Seely et al. (2023) evaluated two DL architectures for forest attribute regression in a temperate mixed forest: the point-based Dynamic Graph Convolutional Neural Network (DGCNN) and the voxel-based Octree Convolutional Neural Network (OCNN). Their results show that while both DL methods outperformed Random Forests, the voxel-based OCNN achieved the lowest prediction errors and reduced mean absolute percentage error. Oehmcke et al. (2024), in their study on airborne LiDAR biomass estimation over Danish national forests, adapted and compared three distinct DL architectures for regression: the point-based PointNet, the point-based Kernel Point Convolution (KPConv), and the voxel-based Minkowski convolutional neural network. Among these, the voxel-based Minkowski CNN consistently outperformed both point-based alternatives across all forest attributes and evaluation metrics. Both studies highlight that (i) voxel-based architectures exhibit greater robustness to variations in forest type, (ii) reliable predictions are conceivable by training a DL model with multi-annual NFI and LiDAR data that may not be fully temporally aligned.

In this paper, we propose a generic deep-learning solution, dubbed **FLORA** (Forest LiDAR Octree Regression with Auxiliary data), for estimating forest attributes at a national-level, that can handle a large diversity of both forest and LiDAR data conditions usually encountered at national scales. **FLORA** is a voxel-based approach designed to estimate forest structural attributes from heterogeneous LiDAR data, validated over France where large-scale NFI and LiDAR data are jointly available. The proposed data does not have counterpart of this size so far (Wegen et al., 2025). Our model predicts six attributes commonly derived from LiDAR data (Coops et al., 2021). We focused here on the following six : dominant height, total volume, *deciduous* stand volume, *coniferous* stand volume, stem density, and basal area. Model performance was evaluated using the rRMSE (%) and the coefficient of determination (R^2), which measure prediction error and explained variance, respectively. This work addresses three main objectives. We first investigate whether a

single DL model trained on data acquired under contrasting phenological conditions (leaf-on and leaf-off) can generalize across seasons as compared to models trained with season-specific data , and whether this robustness holds across forest types. We then examine the specific contribution of overlapping plots, surveyed under both leaf-on and leaf-off conditions, as a training strategy that anchors the model to paired observations of the same forest under varying acquisition contexts. Finally, we assess the added value of auxiliary contextual variables in improving prediction accuracy across heterogeneous acquisition conditions.

2. Materials and methods

2.1. Data

Our approach perform at plot-level and is framed to handle a large diversity of context, has found in the French mainland territory. The advantages are two-fold: this ensures (i) a large amount of data and (ii) significant diversity, therefore capturing very heterogeneous behaviors necessary for our generalization task.

2.1.1. Study area

French forests cover approximately 17.5 million hectares, representing about 32% of the land area of mainland France (Vidal et al., 2016). They are predominantly composed of broadleaved species, with around 68% of the forest areas consisting of deciduous stands. Forest ownership is largely private, as nearly three quarters of forest land is privately owned. In terms of stand structure, more than half of French forests consist of mixed stands, combining either different broadleaved species or mixtures of broadleaved trees and conifers, while pure coniferous stands are less frequent. In metropolitan France, forests contain nearly 190 different tree species, distributed among seven main species: oak, beech, chestnut, maritime pine, Scots pine, spruce, and fir (IGN, 2025).

This structural and compositional diversity is closely linked to the high climatic and topographic heterogeneity of France, which includes oceanic, continental, Mediterranean and mountainous climates. As a result, French forests display a wide range of forest types and structures (Bontemps et al., 2019; Kalinicheva et al., 2025).

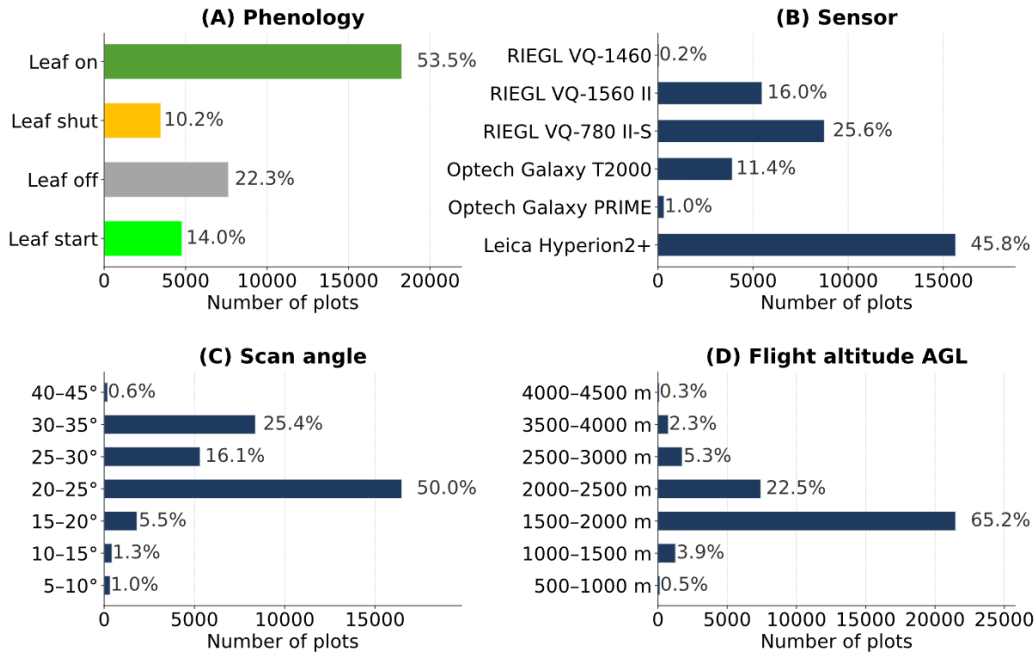


Fig. 1: Variability of our plot-level LiDAR dataset in terms of phenology, sensor, scan angle and, flight altitude. *AGL* stands for *Above Ground Level*.

2.1.2. LiDAR data

We benefit from the large scale 3D airborne LiDAR data acquired in the framework of the French National LiDAR HD program, started in 2021 for a 5 years duration. The objective of the program is to acquire and release in open access LiDAR data over the metropolitan area and ultramarine territories, with the exception of French Guyana, with a point density of at least 10 pulses/m². Such a pulse density was selected to fulfill spatial sampling requirements for both Digital Terrain Model (DTM) generation, land-cover mapping and statistical tasks (Gaydon and Roche, 2025), reaching sometimes 40 pts/m². To achieve such a large multi-year campaign, the territory was divided into 50 km×50 km patches, which were each attributed to one of the six selected private companies or to IGN. Acquisitions were conducted throughout the year, with survey parameters adapted to the relief and the LiDAR device. Several LiDAR systems were employed, with varying emitted energy, pulse rate and operated under multiple flight heights, plane speed and scan angle ranges (Fig. 1). In addition, without inter- and intra-annual planning in the survey periods (*e.g.*, based on forest management or land-

scape consistency), adjacent patches may have been acquired by different companies, under different seasons, and distinct years. Edge effects between patches are reduced by integrating an overlap region of 2-5 km in which at least two surveys were performed.

Fig. 1 shows our dataset exhibits a significant heterogeneity in terms of season and LiDAR surveys, leading in very distinct samplings of the tree canopy and the vegetation underneath.

Raw data processing was mainly performed using automatic routines involving TerraScan software, and classified with Myria3D DL tool (Gaydon, 2022). We used the classified point cloud as the input data for our approach, as it allowed us to directly retain only the ground and vegetation classes and discard the other points, thereby simplifying the preprocessing steps.

2.1.3. French national forest inventory data

The French NFI is based on a systematic sampling of semi-permanent plots distributed across the territory on a 1 km grid. Each year, 1/10 of the grid is explored and around 14,000 plots are surveyed on the field, half of them been visited for the first time, and the other half have been revisited 5 years apart. Quantitative and qualitative data on standing forests and vegetation are collected in the field using concentric circular subplots of 6, 9, 15, and 25 m radius. Stand description is done on the largest plots. Dendrometric data are collected on the three other radius, according to tree diameter: trees with a Diameter at Breast Height (DBH) in the range [7.5 cm – 22.5 cm] are measured on the 6 m radius plot, those in the range [22.5 cm – 47.5 cm] are measured on the 9 m radius plot, and larger trees on the 15 m radius plot. Plot-level estimates of forest attributes are derived on a per ha basis using the probability of inclusion of trees, field measurements as well as allometric models for some variables like volume. In the framework of this research, we relied only on first visit plots and considered the stem density (stems ha⁻¹), the basal area (m² ha⁻¹), the stem volume (m³ ha⁻¹) and its distribution between hardwoods and conifer, as well as dominant height (m).

2.1.4. Our dataset

The study focuses on the mainland territory including Corse. 80% of the territory was covered at the time of this research. We select NFI plots with less than a five-year difference between field measurements and the LiDAR acquisition. This results in a total of 33,877 plots (see Table 1 and Fig. 2), which covers approximately 7.6 million m², that sample most of

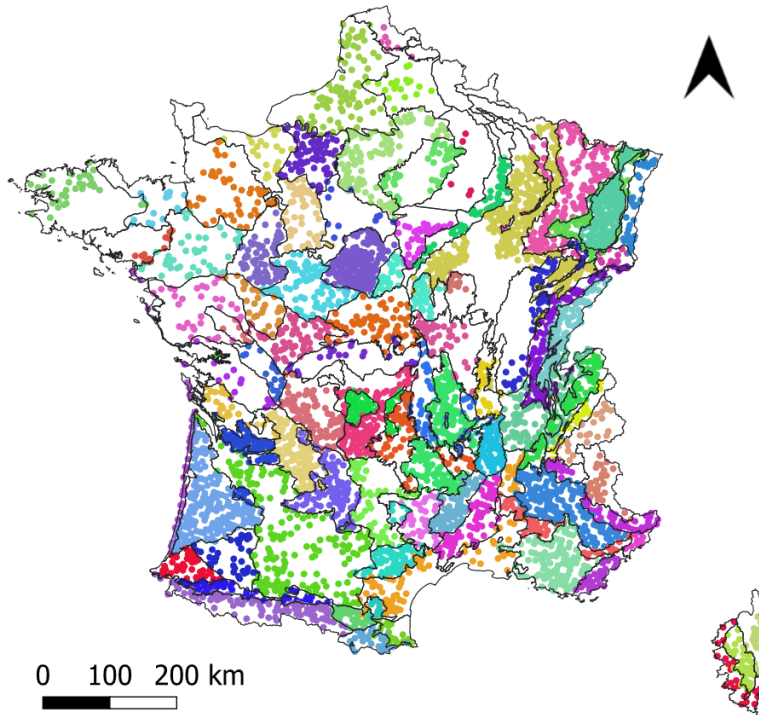


Fig. 2: Spatial distribution over France of the NFI plots used in this study, colored with respect to the sylvo-ecoregion.

the French sylvo-ecoregions (SER), French territory division based on forest ecosystems and management practices. The dataset includes 60 main species, with an average of 502.1 plots having a similar main species (± 901.8 SD). The three most represented species are *pedunculate oak* (4,166 plots), *sessile oak* (3,333 plots), and *European beech* (3,251 plots). We extract LiDAR HD point clouds centered on NFI locations, and link them to the corresponding field measurements. LiDAR point clouds were already classified and a 1 m DTM made jointly available.

We used the LidR package (Roussel et al., 2020) to generate Canopy Height Models (CHM) and to extract point clouds for each plot. To ensure data quality, we applied a three-step filtering procedure, retaining 32,052 plots (93.6% of the initial dataset).

- Plots with a CHM containing more than 10% of missing values were excluded: we discard plots only partially covered by the LiDAR acqui-

sition.

- Plots with large deviations occurring between the field campaign and the LiDAR acquisition were removed. This is likely to reflect stand disturbances, *e.g.*, harvesting or windthrow. We compared the canopy cover fraction derived from the CHM against the one recorded during field surveys as a qualitative estimate of the canopy cover by class of 10%. Plots exhibiting a discrepancy exceeding $\pm 2\sigma$ of the observed distribution of differences were discarded. The canopy cover was defined in the LiDAR data as the proportion of pixels with height above 2 m, a threshold widely used in the literature to separate low vegetation from actual canopy returns (Narine et al., 2023; Rodes-Blanco et al., 2023), and then scaled to the definition of the NFI in 10% classes.
- Stand disturbances was also considered from another perspective. We compared the 95th percentile of CHM heights (H_{95}) to the dominant height measured in the field (H_d). The distribution of residuals $H_{95} - H_d$ is positively skewed: we applied an asymmetric rejection criterion: plots were excluded if $H_{95} - H_d < -2\sigma$ or $H_{95} - H_d > +3\sigma$, where σ denotes the standard deviation of the residual distribution ($\sigma = 3.89$ m). The stricter lower bound reflects the fact that a strong underestimation of H_{95} relative to H_d is most likely indicative of disturbances between the two acquisition dates, rendering the plot unsuitable for model training. Conversely, moderate overestimation of H_{95} relative to H_d can arise from legitimate physical sources: steep terrain slopes are known to introduce height errors in CHM normalization (Vega et al., 2014), and a sparse ground point density during DTM interpolation may lead to residual normalization biases, both resulting in inflated canopy height estimates. These artifacts do not necessarily reflect a mismatch between the field survey and the LiDAR acquisition, and we wish to remain as faithful as possible to the field measurements rather than aggressively discarding potentially valid plots. Therefore, overestimation was tolerated up to a wider margin of $+3\sigma$.

2.2. Methods

FLORA is designed to estimate various forest attributes at the plot level using a sufficient diversity of LiDAR point clouds and that should be agnostic to the forest type. This is a regression task that is efficiently handled

Variable	Min	Mean	Max	SD
Volume (m ³ ha ⁻¹)	0.6038	195.5225	1655.0705	159.3474
Deciduous volume (m ³ ha ⁻¹)	0.0000	122.5009	1362.7934	124.9314
Coniferous volume (m ³ ha ⁻¹)	0.0000	73.0216	1613.6613	147.1187
Density (stem ha ⁻¹)	14.1092	745.7198	5363.3736	569.1066
Basal area (m ² ha ⁻¹)	0.3886	24.9230	132.0870	14.6144
Dominant height (m)	2.3000	18.2193	45.5791	7.0199

Table 1: Descriptive statistics of forest attributes under assessment.

with machine learning solutions and that does not require any preliminary individual tree crown detection step (Fan et al., 2026).

2.2.1. Model architecture

Computational strategy. Our problem can be cast as an *harmonization* challenge, it should therefore exhibit a strong generalization ability over space, time, and plot composition. We selected an Octree-based Convolutional Neural Network combined with a High-Resolution Net (OCNN-HRNet) architecture developed by Wang et al. (2017), and already proved effective for forest attribute regression by Seely et al. (2023), while remaining simple. The proposed framework is designed to operate directly on raw point cloud data, as the conversion into octree structures is automatically performed as a preprocessing step prior to model training (Fig. 3). To improve training stability and accelerate convergence, each target variable is normalized to zero mean and unit variance prior to training using a z-score transformation (Ayrey et al., 2021). This is motivated by the large differences in magnitude and variance across the six forest attributes (*e.g.*, volumes are expressed in m³ ha⁻¹ while basal area is in m² ha⁻¹), which would otherwise cause the loss function to be dominated by the highest-variance attributes. Concretely, for each target k , the normalized value is computed as $\tilde{y}_k = (y_k - \mu_k)/\sigma_k$, where μ_k and σ_k are the mean and standard deviation estimated over the training set. This ensures that all attributes contribute equally to the loss during training, regardless of their physical scale or absolute magnitude. Predictions are back-transformed to the original scale before evaluation.

Detailed design. The model architecture begins with feature extraction from octree-based inputs, transforming raw three-dimensional point cloud data into per-node feature representations (Fig. 3 part A). An initial stack of octree convolution and max-pooling layers reduces the spatial resolution while

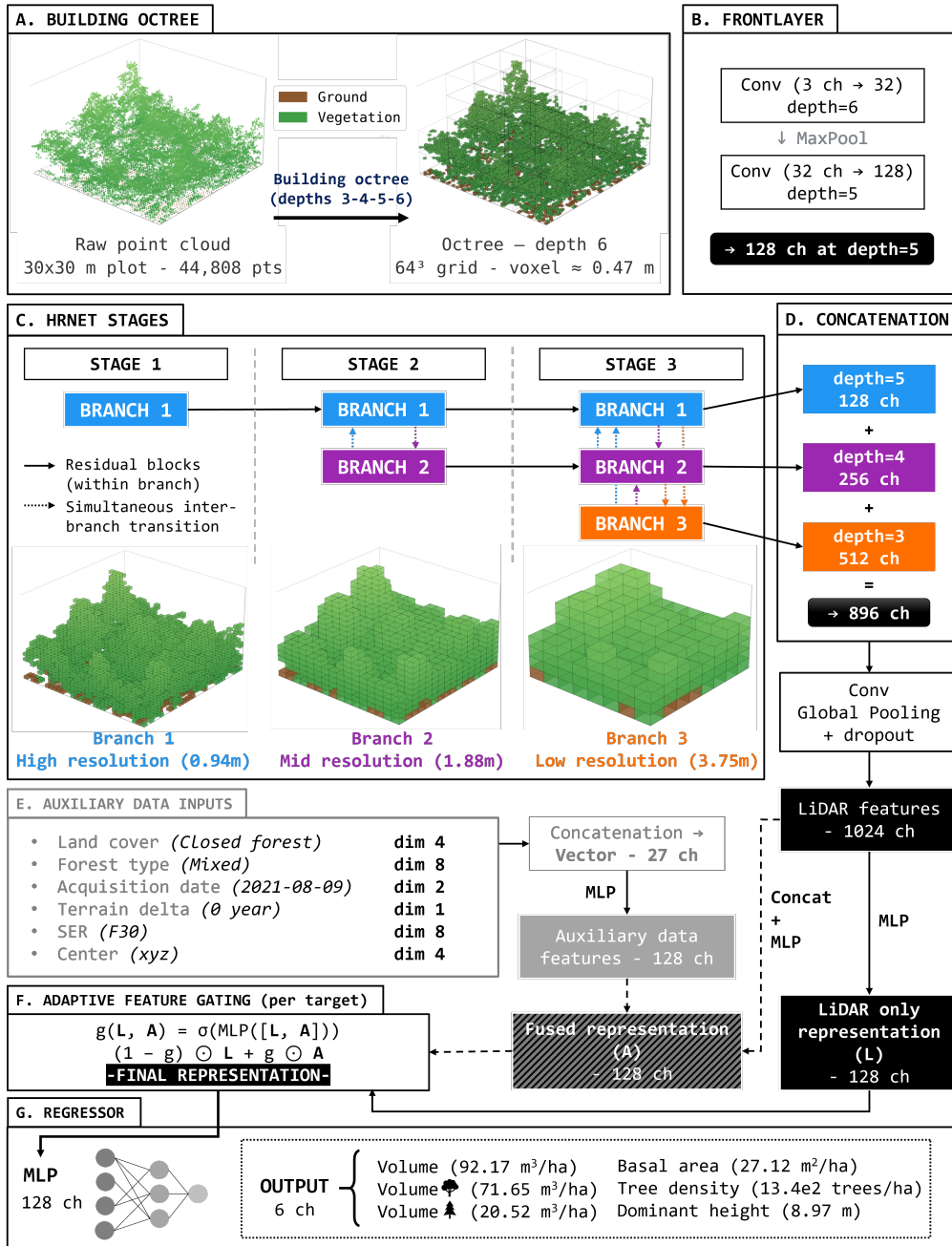


Fig. 3: Step-wise description of FLORA. ch stands for channels, and indicates the size of the feature space at each stage. All provided numbers correspond to the real values for the illustrated plot.

increasing feature dimensionality, producing the first set of feature maps at a coarser octree depth (Fig. 3 part B).

The core of the network follows a HRNet architecture adapted to octree-structured data (Fig. 3 part C). At each stage, parallel branches process feature maps at different octree depths, corresponding to different spatial resolutions, using residual blocks with bottleneck convolutions. The first stage operates on a single high-resolution branch (128 channels). In the second stage, a second branch is introduced at half the resolution (256 channels), and in the third stage a third branch is added at an even coarser resolution (512 channels). Between stages, a transition module simultaneously exchanges information across all branch pairs: each branch receives contributions from all other branches in parallel, computed from the same input state. These contributions are resampled to the target octree depth via successive max-pooling (for higher-resolution sources) or nearest-neighbour upsampling (for lower-resolution sources), with a 1×1 convolution applied when channel dimensions differ, and summed element-wise to form the updated branch input.

After the HRNet stages, the multi-resolution feature maps are concatenated (Fig. 3 part D), resulting in a combined representation of 896 channels ($128 + 256 + 512$). A 1×1 convolution and global pooling layers then aggregate spatial information into a single 1024-dimensional feature vector, with dropout applied for regularization. Finally, in the original model from Seely et al. (2023), a multilayer perceptron regressor composed of two linear layers with ReLU activations processes this vector and outputs the final regression estimates.

We propose several improvements with respect to existing works on deep-based regression of forest attributes : network optimization, increased versatility and context-aware estimation. First, we perform a systematic hyperparameter search to adapt the original architecture to our prediction task. Our six targets are continuous forest structural attributes of heterogeneous scale and ecological meaning: the optimal learning rate, weight decay and batch size may differ substantially from those reported in (Seely et al., 2023) that focuses on above-ground biomass estimation. Second, we design the model to rely exclusively on the 3D spatial coordinates (XYZ) of each point, deliberately excluding intensity and echo-related attributes such as return number, number of returns, and scan angle. Although these features were initially considered, hyperparameter optimization revealed no consistent performance

gains from their inclusion, while intensity measurements were discarded due to the lack of radiometric sensor calibration. Restricting the input to XYZ coordinates also improves robustness across acquisition campaigns by reducing sensitivity to sensor-specific radiometric differences. Finally, we augment geometric information with contextual auxiliary data describing stand-level geographical, semantic, and temporal conditions. We hypothesize that this additional information enables the model to capture ecological and phenological significant variability that is not discernible from point cloud geometry alone. Specifically, we encode (see Fig. 3):

- Geographical-semantic variables (categorical, 20): canopy cover class, composition type, and sylvo-ecoregion using learnable embedding layers.
- Geographical knowledge (discrete, 4): we further include spatial context through a low-dimensional encoding of the plot center location.
- Temporal knowledge (discrete, 3): LiDAR acquisition date is encoded with a cyclic sinusoidal representation (sine and cosine of the day of year), while the temporal gap between the LiDAR acquisition and the field inventory date as a normalized scalar.

Land cover and type of forest formation are obtained from the BD Forêt[®] v2 database. BD Forêt[®] v2 is a vector database describing forest composition over France, and aggregated into 32 main forest formations of pure and mixed compositions. Unlike field-based measurements (*e.g.*, NFI plots), which are highly accurate but spatially sparse, BD Forêt[®] offers wall-to-wall coverage suitable for large-scale modeling. The database includes a hierarchical classification that distinguishes closed and open forests according to canopy cover, as well as poplar plantations, heathlands, and herbaceous formations. Stand composition classes further differentiate pure broadleaf, pure conifer, and mixed forests.

All auxiliary data features are concatenated into a joint vector and passed through a dedicated multi-layer perceptron (MLP) to produce a learned auxiliary data representation in a shared latent space. Rather than modulating geometric features through feature-wise affine transformations like the FiLM method (Perez et al., 2018) (unsuccessful in our case), we adopt a late fusion strategy: the auxiliary data representation is concatenated with the features extracted by the HRNet backbone and jointly processed through subsequent

layers (Fig. 3 part E). To allow the model to adaptively control the contribution of contextual information, we introduce a gating mechanism that learns, for each prediction target, how to interpolate between geometry-driven features and fused representations (Fig. 3 part F).

When the full set of auxiliary data is used, the resulting 27-dimensional representation is concatenated into a single feature vector. We adopt a late-fusion strategy, in which this auxiliary representation is combined with the geometric LiDAR features extracted by the HRNet backbone. To allow the model to adaptively modulate the contribution of contextual information depending on the target variable, we introduce a **target-specific gating mechanism**:

$$\mathbf{g}_k = (1 - g_k) \odot \mathbf{L} + g_k \odot \mathbf{A}, \quad (1)$$

where $\mathbf{L} \in \mathbb{R}^{128}$ denotes the latent representation derived solely from geometric LiDAR features, $\mathbf{A} \in \mathbb{R}^{128}$ corresponds to the fused representation combining LiDAR and auxiliary data. $g_k = \sigma(\text{MLP}([\mathbf{L}, \mathbf{A}])) \in [0, 1]$ is the learned gating coefficient associated with target variable k . When $g_k \rightarrow 0$, the model relies exclusively on LiDAR-derived geometric information, whereas when $g_k \rightarrow 1$, it fully incorporates auxiliary contextual information. This mechanism provides the model with **partial interpretability**, as the distribution of gate values on the test set enables quantification, for each forest attribute, of the relative contribution of contextual information to the final prediction. We hypothesize this design enables the network to selectively leverage auxiliary data when informative, while preserving robustness when such information is noisy or less relevant.

Hyperparameter optimization. DL model performance is highly sensitive to the choice of hyperparameters, such as the learning rate, batch size, and regularization coefficients. Hyperparameter tuning is therefore formulated as an optimization problem in which hyperparameters are selected to minimize a validation loss. Common approaches include grid search, random search, and Bayesian optimization (Raiaan et al., 2024). While grid search evaluates predefined combinations of hyperparameters, random search samples from predefined distributions and is generally more efficient in high-dimensional spaces (Bergstra et al., 2011). Bayesian optimization further improves efficiency by modeling the relationship between hyperparameters and model performance using surrogate probabilistic models. Hyperparameter optimization was performed using Optuna (Akiba et al., 2019), an open-source framework that supports dynamic construction of the search space

during execution. Optuna relies on Bayesian optimization based on a Tree-structured Parzen Estimator, which adaptively samples promising regions of the hyperparameter space. In addition, Optuna integrates pruning mechanisms that enable early stopping of unpromising trials, making it particularly suitable for computationally expensive DL models (Raiaan et al., 2024; Karakutuk et al., 2025). The optimized hyperparameters included the learning rate, batch size, dropout probability and weight decay coefficient. These hyperparameters were selected as they have the greatest influence on optimization dynamics (learning rate, batch size) and generalization (dropout, weight decay). The search space was defined using log-uniform sampling for the learning rate and categorical sampling for the remaining parameters.

The optimization procedure was implemented in two sequential phases. First, a fixed number of trials were executed. Due to the dataset size, 50 trials required 100 hours of computation. Although a more extensive exploration of the hyperparameter space would have been desirable, the high computational cost of this procedure led us to limit the search to 50 trials. Each trial consisted of training the model for a fixed number of epochs of 10 (preliminary results showed that models converge approximately at epoch 7). Candidate configurations were ranked according to their mean validation loss. The top three configurations were then selected for a second evaluation phase. In this phase, each configuration was retrained and validated using a five-fold cross-validation scheme and a larger number of training epochs (20). The final set of hyperparameters was chosen based on the lowest mean validation loss observed during this second phase. This two-stage strategy allows efficient exploration of the hyperparameter space while providing a robust and unbiased estimate of model generalization performance.

2.2.2. Study Design

The research questions outlined in Section 1 are addressed through four complementary experiments, each isolating a specific factor: the effect of phenological conditions on model generalization, the potential confound introduced by class imbalance, the role of overlapping multi-season acquisitions, and the contribution of auxiliary contextual variables together with the interpretability of their integration.

All models introduced below were built upon our **FLORA** architecture (see Section 2.2.1). They were trained in a supervised framework using paired LiDAR point cloud samples and NFI ground truth measurement, for 20 epochs with optimized hyperparameters. Forest type was defined at the plot level

from NFI records, distinguishing deciduous, coniferous, and *mixed* stands. Phenological classes were defined using fixed temporal boundaries applied to acquisition dates (leaf-start: Mar. 15 ; leaf-on: May 15 ; leaf-shut: Sep. 15 ; leaf-off: Nov. 15): leaf-on corresponds to full canopy closure, and leaf-off to the leafless winter period. Transitional stages were excluded to ensure unambiguous class membership. leaf-on and leaf-off acquisitions represent 54% and 22% of the total dataset, respectively.

Experiment 1: All-seasons versus season-specific prediction. We assess whether a single model trained on both phenological seasons generalizes as well as season-specific models. Three independent models were trained: a **leaf-on model** ($n = 14,142$), a **leaf-off model** ($n = 5,675$), and a **full model** combining both seasons ($n = 19,817$). Each season-specific model was evaluated under two conditions: **same-season testing** (the test set matched the training season), and **cross-season testing** (the model was applied to acquisitions from the opposite season). The full model was evaluated on both seasons. To further disentangle the effect of class distribution from that of seasonal coverage, the full model was additionally trained on a balanced dataset enforcing equal leaf-on and leaf-off representation through undersampling of the majority class; the **balanced model** and unbalanced original full model are compared to isolate the contribution of class imbalance (54% leaf-on vs. 22% leaf-off) from that of phenological diversity. For all configurations, samples were split into 70% training, 10% validation, and 20% test, stratified by phenological class and forest type.

Experiment 2: Benefiting from overlapping acquisitions. We quantify the impact of plots surveyed under both leaf-on and leaf-off conditions as a training strategy. Two datasets of equal size were compared: one composed exclusively of overlapping plot pairs (*i.e.*, plots with acquisitions in both seasons), and one restricted to single-acquisition plots. Overlapping plots arise from two sources: spatial overlap between adjacent acquisition blocks, and flight-line sidelap within a single block (when point clouds contained data from multiple flights, points were separated using GPS timestamps). Among the 1,239 NFI plots acquired more than once across the full dataset, only 38 were observed in both phenological seasons, yielding 76 paired acquisitions (38 leaf-on and 38 leaf-off). The single-acquisition dataset was constructed as $K = 3$ disjoint subsamples of equal size, drawn without replacement from the pool of non-overlapping plots, ensuring no plot appeared in more than

one subsample. Both conditions were evaluated on a fixed holdout test set composed exclusively of single-acquisition plots. Performance is reported as mean \pm standard deviation of rRMSE% across the $K = 3$ runs.

Experiment 3: Assessing the contribution of auxiliary contextual information. To assess the contribution of auxiliary data, two models were compared under otherwise identical conditions: our **full model** incorporating ecological and spatiotemporal data, fused via the late-fusion gating mechanism (*Aux*), and a **base model** consisting of FLORA modified to rely solely on LiDAR point cloud features (*No Aux*). The gating coefficient $g_k \in [0, 1]$ learned for each target variable k quantifies the relative contribution of contextual information to the final prediction: values close to 0 indicate the model relies primarily on LiDAR-derived geometric features, while values close to 1 indicate a dominant contribution from auxiliary data. Since the gates are initialized at 0.5, values remaining close to this midpoint suggest that the auxiliary information neither contributed positively nor negatively in a substantial way. Analyzing the distribution of gate values on the test set thus provides a form of partial interpretability, enabling us to characterize, per forest attribute, how much the model draws on contextual information. This is complemented by an ablation protocol in which individual auxiliary variables are successively selected to quantify their marginal contribution. Both model variants were optimized independently using Optuna (50 trials), with the best hyperparameter configuration selected by five-fold cross-validation based on the lowest mean validation loss.

3. Results

3.1. Hyperparameter tuning

Hyperparameter optimization revealed that integrating auxiliary data fundamentally reshapes the optimization landscape, requiring a learning rate 3.5 times smaller, half the batch size, and double the dropout rate compared to the base model, while simultaneously demonstrating greater representational richness through resilience to aggressive regularization.

This part shows the results of the hyperparameter optimization using the aforementioned setup, conducted independently for the base model and the full model. Notably, the two variants converged to markedly different configurations, which reflects the impact of auxiliary data on the model’s learning dynamics. The learning rate converged to a value approximately

3.5 times lower in the auxiliary model (4.457×10^{-4} vs. 1.570×10^{-3}), reflecting the more complex loss landscape induced by the fusion of heterogeneous information sources: the gating mechanism must learn to balance two complementary streams and is consequently more sensitive to large gradient steps. The optimal batch size likewise **halved** (16 vs. 32): smaller batches produce noisier gradient estimates that tend to converge towards flatter, more generalizable minima (Keskar et al., 2017). This is particularly beneficial here as the auxiliary metadata introduces a combinatorial diversity of input configurations (*e.g.*, rare sylvo-ecoregion and acquisition period combinations), encouraging the model to find solutions that generalize across this expanded input space rather than overfitting to the most frequent covariate patterns. The most striking difference concerns the dropout rate, which **doubled** when auxiliary data was introduced (0.6 vs. 0.3): rather than viewing this solely as a defensive regularization measure, this result can be read as evidence of the representational richness brought by auxiliary data: the model remains performative despite a substantially higher fraction of masked activations, suggesting that the auxiliary features provide sufficiently redundant and complementary signals for the network to tolerate aggressive information dropout, while simultaneously preventing the model from short-circuiting point cloud processing by treating high-level contextual features, such as forest type, geographic region, or acquisition date, as direct proxies for the target variable. Conversely, weight decay was **reduced by a factor of approximately three** (3.6×10^{-5} vs. 1×10^{-4}): since the stronger dropout already provides substantial regularization, a lower ℓ_2 penalty avoids over-constraining the learnable embeddings associated with categorical metadata, which require sufficient parametric freedom to encode meaningful distinctions between categories. Taken together, these results paint a coherent picture of how auxiliary data reshapes the optimization problem: it substantially enriches the representational space, as evidenced by the model’s resilience to aggressive dropout, while the added complexity of multimodal fusion calls for more conservative gradient updates, and the combination of smaller batches and reduced weight decay ensures that this richer representation generalizes effectively across the full diversity of input configurations.

3.2. All-seasons versus season-specific prediction

3.2.1. Results for full model

Metric	Leaf-on test		Leaf-off test		All test	
	rRMSE	R ²	rRMSE	R ²	rRMSE	R ²
Volume	40.83	0.76	36.21	0.67	39.28	0.736
Conif. Vol.	53.95	0.75	43.09	0.69	49.72	0.742
Decid. Vol.	77.23	0.82	96.25	0.83	81.99	0.821
Density	53.72	0.47	57.44	0.42	54.82	0.460
Basal Area	36.81	0.56	34.03	0.48	36.03	0.544
Height	12.81	0.89	11.44	0.81	12.33	0.884

Table 2: **Full model tested separately on leaf-on, leaf-off, and complete datasets;** results for the three forest types (Coniferous, Deciduous and Mixed; see details in Appendix A).

The full model achieves strong performance on height and total volume, while stem density remains the most challenging attribute ($R^2 < 0.47$), with species-specific volume predictions exhibiting high variability across forest types.

Table 2 presents the global performance of the full model across all forest plots, evaluated on both leaf-on and leaf-off test sets. Details for forest types are provided in Appendix A.

Height is the best-predicted attribute by a large margin, with error below 13% and $R^2 > 0.89$ on leaf-on, and remains stable across forest types. Total volume also yields strong results (error $\approx 40\%$, $R^2 = 0.76$ on leaf-on), with consistent performance across forest types. Basal area achieves moderate accuracy (error $\approx 36\%$, $R^2 = 0.56$ on leaf-on), while stem density is the most poorly predicted attribute, with R^2 below 0.47 on both test sets.

Predictions for the proportion of deciduous and conifers exhibit the highest errors and the widest per-forest-type variability. Coniferous and deciduous volumes reach errors of 53.95% and 77.23% on leaf-on respectively, with extreme rRMSE values on ecologically mismatched forest types (*e.g.*, deciduous volume on coniferous plots), where target values are near zero. R^2 values nonetheless remain relatively high for deciduous volume (0.82–0.83), reflecting good rank-order predictions despite high absolute errors.

With the exception of density, and volume of deciduous, other attributes leaf-off errors are generally lower than or comparable to leaf-on, while R^2

values tend to be higher on leaf-on. This trend indicates that leaf-on capture better their overall variance, but is impacted by larger prediction errors.

When evaluated on the combined *All test* dataset, performance remains highly consistent with the separate leaf-on and leaf-off evaluations, with only marginal changes in both rRMSE and R^2 across all targets. Overall trends observed in the separate test sets are preserved, with height and total volume remaining the most accurately predicted, while stem density and species-specific volume fractions continue to be the most challenging targets.

3.2.2. *Balanced*

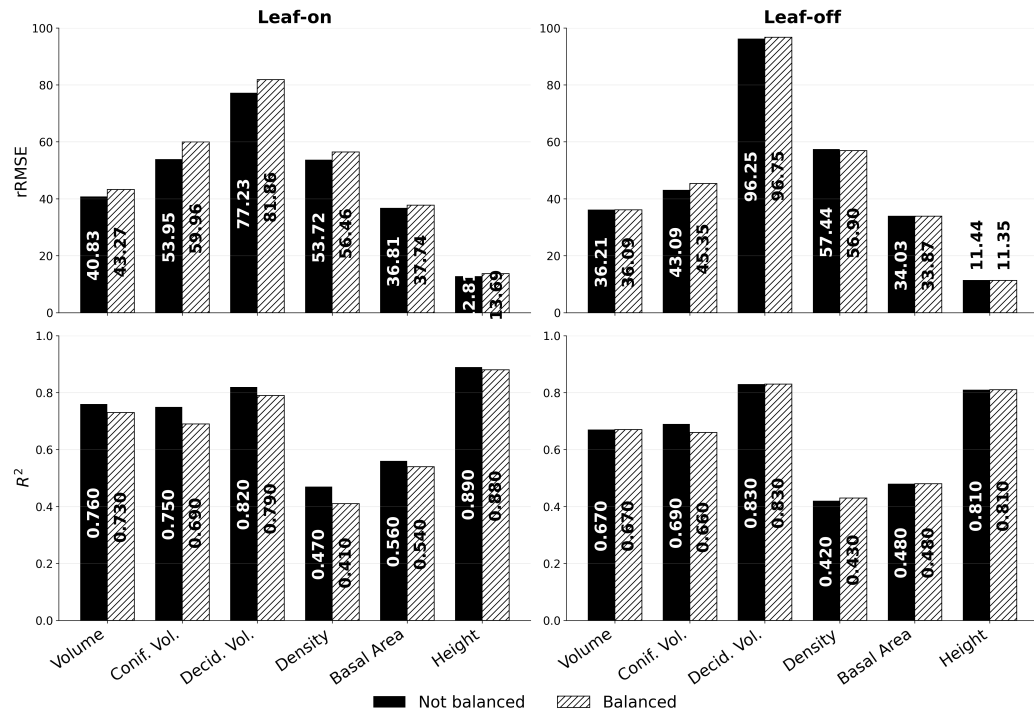


Fig. 4: Comparison of predictive performance between the full model (solid black bars) and the balanced model (hatched bars) across all target forest attributes. Results are reported for rRMSE (%) and R^2 on leaf-on and leaf-off test sets.

Balancing the training set leads to moderate performance degradation on leaf-on while largely preserving leaf-off performance, suggesting that the original training imbalance does not critically bias the full model.

Figure 4 compares the full and balanced models across all target attributes. Balancing the training set leads to a moderate degradation of leaf-on performance across most attributes, while leaf-off performance is largely preserved or marginally improved. The effect is most pronounced for coniferous volume and stem density, where leaf-on error increases by 6 and 3 points respectively, and for height, where leaf-on R^2 drops from 0.890 to 0.880. In contrast, height and basal area show the smallest sensitivity to the balancing strategy, with differences below 1 point of error on both test sets. Overall, the performance gap between balanced and unbalanced models remains limited, suggesting that the initial imbalance does not critically bias the full model. Detailed per-forest-type results are reported in Appendix B.

3.2.3. Season-Specific Models

Metric	Leaf-on model				Leaf-off model			
	Same-season		Cross-season		Same-season		Cross-season	
	ΔrRMSE	ΔR^2	ΔrRMSE	ΔR^2	ΔrRMSE	ΔR^2	ΔrRMSE	ΔR^2
Volume	+0.97	-0.01	+3.22	-0.07	+3.46	-0.07	+24.32	-0.38
Conif. Vol.	+3.54	-0.03	+7.24	-0.11	+10.94	-0.18	+45.13	-0.38
Decid. Vol.	+6.87	-0.04	+33.15	-0.14	+22.52	-0.09	+119.06	-1.01
Density	+0.43	-0.01	+5.93	-0.13	+1.23	-0.03	+14.07	-0.32
Basal Area	+0.98	-0.02	+3.74	-0.12	+1.76	-0.06	+19.47	-0.40
Height	+1.17	-0.02	+0.78	-0.03	+4.64	-0.18	+5.79	-0.03

Table 3: Difference in performance between season-specific and full models. $\Delta\text{rRMSE} = \text{rRMSE}(\text{seasonal}) - \text{rRMSE}(\text{full})$; $\Delta R^2 = R^2(\text{seasonal}) - R^2(\text{full})$, where the full model reference is always evaluated on the same test set as the season-specific model.

Season-specific models consistently underperform the full model even within their calibration domain, with cross-season generalization exhibiting strong asymmetry: the leaf-on model transfers reasonably well to leaf-off data, while the leaf-off model degrades severely when applied to leaf-on acquisitions.

Table 3 compares season-specific and full model performance under same-season and cross-season evaluation. The full model has better performance than the seasonal one when ΔrRMSE is positive and ΔR^2 negative.

Same-season performance. Models trained on either leaf-on or leaf-off data show slightly lower performances than the full one for both rRMSE and R^2

(Tab. 3). This trend applies to both leaf conditions, indicating that the full model performs better than the specific ones, even in their calibration domain. For leaf-on, differences remain modest: volume error increases by less than 1 point (41.80% vs. 40.83%), and stem density and basal area stay within 1% of the full model. The degradation is more visible for coniferous volume (57.49% vs. 53.95%) and deciduous volume (84.10% vs. 77.23%).

On leaf-off, the gap widens. While basal area and stem density remain comparable (35.79% vs. 34.03% and 58.67% vs. 57.44%), deciduous volume shows a pronounced degradation (118.77% vs. 96.25%) and height drops substantially in both error and explained variance (16.08%, $R^2 = 0.626$ vs. 11.44%, $R^2 = 0.811$), suggesting that training on a single season is particularly limiting for structurally sensitive attributes.

Cross-season performance. Cross-season generalization is strongly asymmetric between the two seasonal models. On one hand, the leaf-on model applied to leaf-off acquisitions maintains acceptable performance for most attributes: The rRMSE of volume increases by 3.22% and R^2 decreases by 0.07, staying close to same-season performance, and height remains robust with less than 1% error difference. The main degradation in error is observed for deciduous volume (+33.15%) and coniferous volume (+7.24%). On the other hand, the leaf-off model applied to leaf-on acquisitions degrades severely across all attributes. Volume rRMSE increases by 24.32%, coniferous volume by 45.13%, and deciduous volume collapses by 119.06%. Basal area R^2 drops by 0.4 and stem density R^2 by 0.32, while height, though degraded in error (+5.79%), partially retains its R^2 (-0.03). This asymmetry suggests that leaf-off acquisitions carry less transferable structural information than leaf-on data when applied outside their training distribution.

Comparison with the full model. The full model consistently outperforms season-specific models in both settings. In same-season testing, its advantage is clearest on leaf-off, where it reduces volume error by more than 3 points and nearly halves the height error gap (11.44% vs. 16.08%, $R^2 = 0.811$ vs. 0.626). In cross-season testing, the full model avoids the severe degradation of the leaf-off-specific model: it maintains volume error at 40.83% on leaf-on where the leaf-off-specific model reaches 65.15%, and preserves R^2 above 0.75 for volume and height across both test sets. per-forest-type results are reported in Appendix C.

3.3. Can we benefit from overlapping acquisitions ?

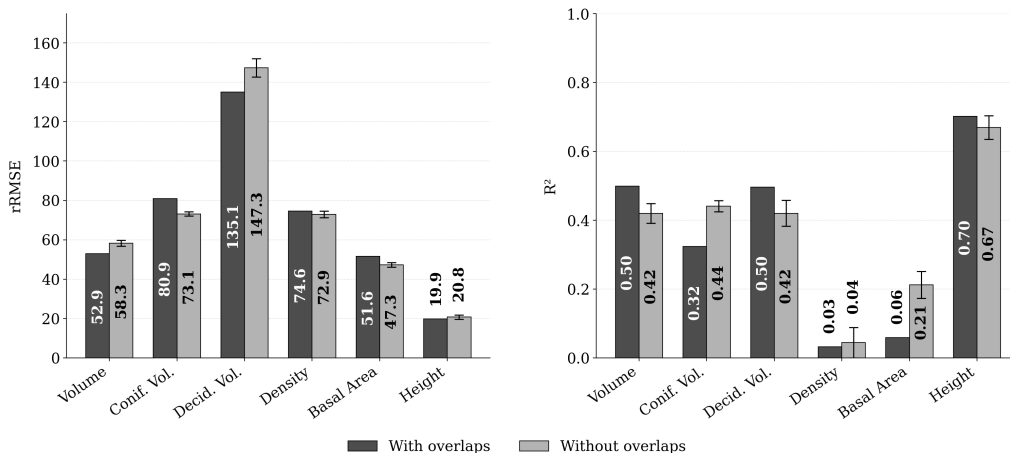


Fig. 5: Effect of spatial overlap between LiDAR acquisitions on model performance. Metrics (rRMSE and R^2) are compared for overlapping vs. non-overlapping areas, averaged across all species. Values for non-overlapping areas represent mean \pm standard deviation over K runs.

Spatial overlap between LiDAR acquisitions produces contrasting effects depending on the target attribute: volumetric estimation improves substantially for total and deciduous volume, while coniferous volume, basal area, and density degrade, and height remains largely unaffected.

Overlapping acquisitions yield contrasting effects depending on the target attribute (Figure 5 and Appendix D). Performance improves most clearly for total and deciduous volume, with rRMSE reductions of roughly 5 and 12 points respectively, suggesting that the complementary seasonal information captured by paired acquisitions benefits volumetric estimation of broadleaf stands. Coniferous volume shows the opposite trend, with rRMSE increasing from 73.15% to 80.87% and R^2 dropping from 0.441 to 0.324. Basal area and density also degrade under the overlap condition, while height remains largely unaffected in either direction. Compared to the full model, results in this experiment are strongly degraded for all target variables (*e.g.*, $\approx +10$ points in volume error) probably due to the reduced train dataset size.

3.4. Do auxiliary contextual information bring additional knowledge ?

Auxiliary data yield limited improvements across most attributes, with species-specific volumes showing the highest gate activations and largest rRMSE

reductions, while height demonstrates no improvement linked to auxiliary data and density systematically degrades.

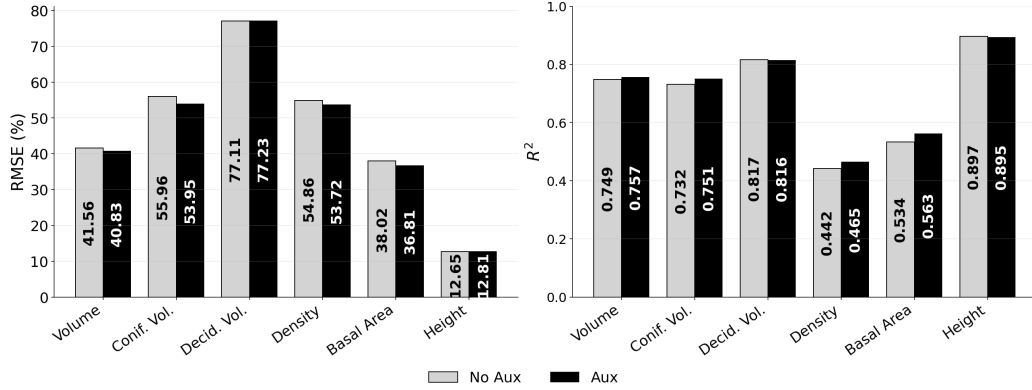


Fig. 6: Barplots showing changes in rRMSE and R^2 between the LiDAR-only baseline (No Aux) and FLORA (Aux).

Impact on predictive accuracy (Figure 6). Figure 6 compares global rRMSE and R^2 obtained with LiDAR-only inputs (grey bars) to the FLORA architecture including auxiliary data (black bars), both trained on the full training set. Detailed numerical results are provided in Appendix A. Across attributes, changes remain moderate in absolute magnitude, but clear patterns emerge. For **total volume**, rRMSE decreases by approximately 0.7%, while R^2 remains stable. Coniferous volume shows slightly larger effects, with rRMSE reductions of 2% and R^2 gains reaching +0.02 while performance on deciduous volume are stable. Basal area (rRMSE -1.21, R^2 +0.03) and Density (rRMSE -1.14, R^2 +0.02) exhibit small improvements. In contrast, height show minimal sensitivity to auxiliary data: rRMSE variations remain under 0.2%, with R^2 changes below 0.01. Overall, auxiliary data lead to limited improvements, but more noticeable for species-specific volume components.

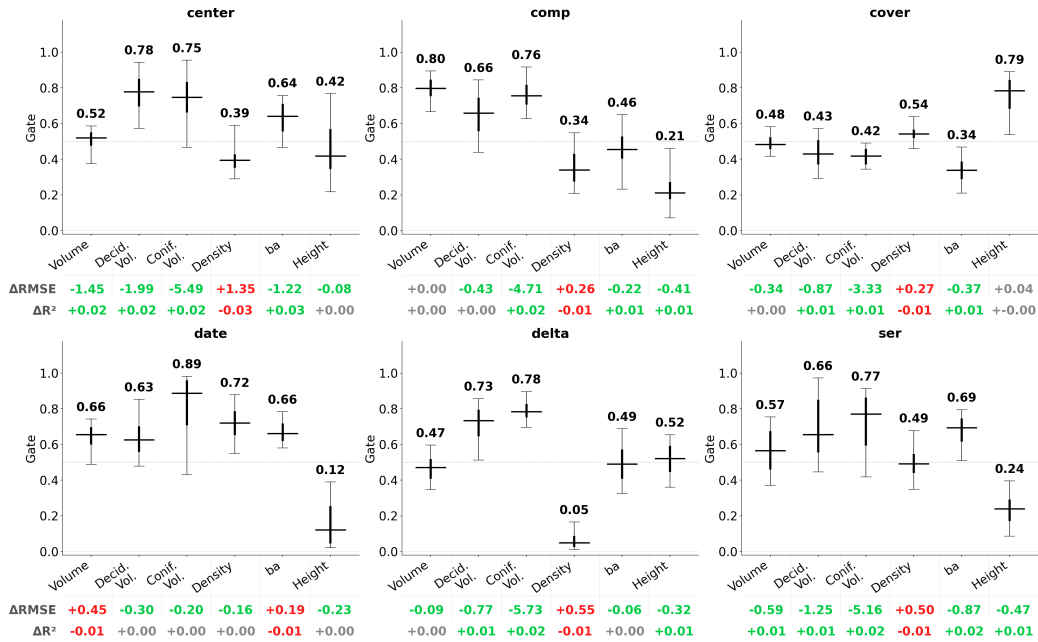


Fig. 7: Distribution of learned gating coefficients for each auxiliary data configuration (Config) across target forest attributes. For each configuration, whiskers represent the 5th–95th percentile range, thick vertical segments indicate the interquartile range, and horizontal black lines denote median gate values. The dashed horizontal line marks $g = 0.5$. Values reported below each panel show relative performance differences with respect to the LiDAR-only baseline ($\Delta = \text{Config} - \text{No_Aux}$), expressed as changes in rRMSE (%) and R^2 . Green and red values respectively denote positive and negative variations according to the corresponding metric convention.

Figure 7 reports the median gate values and associated performance differences for each auxiliary variable and target attribute. Full results are reported in Appendix E.

Species-specific volumes benefit most from auxiliary information. Coniferous volume consistently exhibits the highest gate activations across all configurations (0.66–0.89), regardless of which variable is provided, with rRMSE reductions reaching -5.73 for the time `delta` between LiDAR and field acquisition alone and -6.20 for the full auxiliary set. Deciduous volume follows a similar pattern, with gate values between 0.63 and 0.78 and consistent improvements up to -1.99 points for `center`. Total volume and basal area show intermediate activations (≈ 0.47 – 0.66) and more modest but generally positive contributions. Height displays the most heterogeneous gating behavior, ranging from 0.12 (`date`) to 0.79 (`cover`), yet without consistent performance

benefit, high gate values do not systematically translate into lower error, suggesting the model gates toward auxiliary data without effectively exploiting it for this attribute. Density is the only attribute for which auxiliary information systematically degrades performance across configurations, with rRMSE increases up to +1.35 for `center`, despite gate values remaining near 0.5.

Among individual variables, `center` and `delta` yield the strongest marginal contributions for volume-related attributes, while `date` and `cover` have negligible or inconsistent impact across most targets.

4. Discussion

4.1. Full model performance

The full model achieves competitive results for height and total volume, which are the best-predicted attributes across all configurations (rRMSE < 13% and $R^2 > 0.88$ for height; rRMSE $\approx 39\%$ and $R^2 = 0.74$ for total volume on the combined test set). For height, these results are consistent with recent studies using ALS data at national scale in Sweden: Nilsson et al. (2017) report stand-level rRMSE of 9.8–11.2% using linear regression on 11,500 NFI plots, and Björnberg et al. (2026) report approximately 10–12% using XGBoost and CNN on NFI plots. The differences on total volume is more pronounced: at the local scale, Hawryło et al. (2020) report rRMSE of 24.16–31.69% over 360 stands within a single Polish forest district using ALS combined with Landsat composites and various machine learning methods, while at the national scale, Nilsson et al. (2017) report rRMSE of 17.2–22.0% and Björnberg et al. (2026) approximately 30%. Both papers were conducted on Swedish boreal forests where Norway spruce and Scots pine together account for approximately 80% of standing volume. Conversely, our dataset comprises 33,877 NFI plots spanning 60 main species with $\approx 72\%$ of plots dominated by deciduous stands, making national-scale prediction substantially more challenging.

This spatial contrast is further supported by Miettinen et al. (2025), who show strong regional variability in Sentinel-2 kNN-based forest estimates over 151,000 NFI plots across 14 European countries divided in multiple ecological zones. In the area including Swedish boreal reference region, model performance is consistently higher than in most other areas, with rRMSE of 58.2% for volume, and moderate predictive skill ($R^2 = 0.54$). In contrast, areas covering the French territory exhibit systematically higher errors, with

volume rRMSE ranging from 61.7% to 74.6% confirming the impact of forest structure and composition on performance.

For basal area, our global results (rRMSE \approx 36.0%, $R^2 = 0.54$ on the combined test set) align reasonably with recent literature. Keskes et al. (2025) in Romania report, at 10 m resolution, an R^2 of 0.28–0.35 and rRMSE of 21.7–32.3%. Over Sweden, Nilsson et al. (2017) achieve rRMSE ranging between 20.4–26.7%. At an even larger scale, Matasci et al. (2018) mapped structural attributes across the 552 million hectares of Canadian boreal forest using 30 m annual Landsat composites (1984–2012 time series) combined with LiDAR plots from a national transect survey and a kNN-Random Forest imputation approach, reporting $R^2 = 0.544$ and rRMSE of 50.7% for basal area. Our results, obtained with national scale high-density LiDAR, thus compare favourably with large-area mapping studies relying on coarser remotely sensed data, while remaining above the accuracy levels reported for local or compositionally simpler settings.

Stem density is the most poorly predicted attribute across all configurations (RMSE \approx 55%, $R^2 < 0.47$), a result consistent with the broader literature. For example, in a subtropical planted forest in southern China, Liu et al. (2021) found that stem density was among the most challenging forest structural parameters to estimate from airborne LiDAR data, despite using a hybrid deep-learning model (Deep-RBN) that outperformed conventional approaches. Stem density predictions exhibited substantially lower accuracy than estimates of tree height and volume, with an rRMSE = 20.34%–31.03% and $R^2 = 0.52$ –0.72 under the optimal model configuration. In the two studies focusing on high-density ALS in New Zealand plantation forests of *radiata pine*, stem density consistently yields the lowest performance among all forest attributes considered. Using standard ALS metric-based regression models, Pearse et al. (2018) report a R^2 of 0.48 and rRMSE of 34% for stand density, compared to 0.88 for mean top height, noting explicitly that ALS models produced poor estimates of stand density. Similarly, using Random Forest regression, Leonardo et al. (2020), in the southeast of New Zealand, achieve an R^2 of 0.47 and rRMSE of 32.3% for stem density, versus 0.86 for height. Unlike height or volume, stem density is strongly influenced by stand history, thinning regime, and understorey structure-information that is poorly encoded in plot-level point cloud geometry and that auxiliary data cannot fully compensate for, as further evidenced by Irulappa-Pillai-Vijayakumar et al. (2019), who attribute the comparatively poor density predictions of their k-NN model to the structural complexity of broadleaved-dominated

forests in central France.

To our knowledge, no existing study has directly predicted absolute coniferous and deciduous volumes as separate target variables. The closest comparable work is that of Miettinen et al. (2025), who produced Pan-European maps of deciduous-coniferous proportion (DCP). While their DCP metric provides the proportion of conifers (allowing broadleaf proportion to be derived as $100 - \text{DCP}$), the absolute volumes of each species group remain unquantified. In the French territory covered by their study, the rRMSE for conifer proportion ranged from 61.8% to 71.6% on the processing area corresponding to France. This finding underscores the inherent difficulty of species-specific attribution. Our results for coniferous volume (RMSE \approx 50%, $R^2 = 0.74$) and deciduous volume (RMSE \approx 82%, $R^2 = 0.82$) showcase the challenging task of predicting absolute species-specific volumes. Despite the high error values, the R^2 metrics remain reasonably strong, suggesting that the models capture spatial variability and stand composition patterns well despite substantial prediction errors at the plot level.

4.2. Effect of balanced training

Balancing the training set to equalize the representation of leaf-on and leaf-off acquisitions leads to a moderate and selective degradation of performance. On leaf-on test data, most attributes show slightly higher errors under the balanced configuration, most notably for coniferous volume (+6 points rRMSE) and stem density (+3 points), while leaf-off performance is largely preserved or marginally improved (Table in Appendix B). Height and basal area show the smallest sensitivity to balancing, with differences below 1 point on both test sets (Figure 4). This pattern is consistent with the composition of the original dataset: leaf-on acquisitions represent the majority of plots, so balancing effectively down-samples the dominant season and reduces the model’s exposure to the most frequently occurring acquisition context. The limited overall impact suggests that the original imbalance does not critically bias the full model, and that the unbalanced configuration is preferable for operational use given its better exploitation of available training data. This is consistent with findings in class-imbalanced learning more broadly, where down-sampling the majority class tends to improve minority-class performance but at the cost of overall accuracy (Japkowicz and Stephen, 2002)

4.3. Phenological robustness and season-specific generalization

The results presented in Tables 3 and Appendix C address two complementary questions: whether season-specific models outperform the full model on their own acquisition season, and whether they generalize adequately to the opposite season.

4.3.1. Same-season performance and the advantage of leaf-off

In same-season evaluation, the leaf-off model achieves lower rRMSE than the leaf-on model for most volumetric attributes (*e.g.*, total volume: 39.67% vs. 41.80%), consistent with the literature showing that leaf-off acquisitions generally yield more accurate volume estimates due to greater canopy penetration and improved ground sampling (Villikka et al., 2012; White et al., 2015). This advantage is however attribute-dependent: height estimation degrades substantially under leaf-off same-season conditions (16.08% vs. 13.98% for the leaf-on model), likely because the absence of foliage reduces the contrast between canopy strata and lowers the upper return density that drives height predictions. This is consistent with findings by Davison et al. (2020), who show that leaf-off conditions shift the return distribution toward lower canopy levels, particularly in deciduous stands.

The leaf-off model also shows marked degradation for deciduous volume in same-season evaluation, with rRMSE dropping from 118.77% to values exceeding 150% without auxiliary data. This reflects a well-known difficulty: under leaf-off conditions, mixed stands containing both deciduous and evergreen species present ambiguous return distributions, as retained conifer foliage introduces structural noise that complicates the separation of species-specific contributions (Villikka et al., 2012). White et al. (2015) report similar patterns, noting that leaf-off models show larger errors for deciduous volume attributes, particularly for merchantable volume, where rRMSE can differ by up to 7% between leaf conditions.

4.3.2. Cross-season generalization and asymmetric transferability

Cross-season generalization is strongly asymmetric. The leaf-on model applied to leaf-off acquisitions maintains acceptable performance for most attributes: total volume reaches 39.43% rRMSE ($R^2 = 0.60$), close to its same-season performance, and height remains robust at 12.22% ($R^2 = 0.78$). By contrast, the leaf-off model applied to leaf-on acquisitions degrades severely: total volume increases to 65.15% ($R^2 = 0.38$), coniferous volume to 85.96%, and deciduous volume collapses to 196.29% ($R^2 = -0.19$). This asymmetry is

consistent with White et al. (2015), who report that applying leaf-off models to leaf-on data on eight forest attributes (top height, mean height, Lorey’s mean height, basal area, quadratic mean diameter, merchantable volume, total volume, and total aboveground biomass) results in average absolute rRMSE increases of 16.8% for coniferous stands and 25.8% for deciduous stands, and with Villikka et al. (2012), who observe that a leaf-off model applied to leaf-on deciduous plots yields rRMSE exceeding 70% and bias approaching 50%. The physical explanation is straightforward: a model trained on leaf-off point clouds, where returns are concentrated in the lower canopy and on the ground, lacks the representational capacity to interpret the denser and higher return distributions, representative of leaf-on acquisitions (Ørka et al., 2010).

4.3.3. Practical implications for acquisition planning

These results raise a practical question for operational forest inventory: when is it preferable to acquire leaf-on versus leaf-off data? The answer depends on the intended application. Leaf-off acquisitions are generally preferred for terrain modeling and archaeological prospection, where reduced foliage improves ground return detection and the visibility of micro-topographic features beneath forest canopies (Simpson et al., 2017; Moudrý et al., 2019). Conversely, leaf-on acquisitions provide a more realistic characterization of canopy fuels and vegetation continuity, making them more suitable for wildfire-related mapping applications (Moran et al., 2020). For multi-attribute forest inventory, our results suggest that leaf-on acquisitions are preferable when cross-season generalization is required, given their superior transferability to leaf-off conditions. However, acquisition season is not always a free parameter: mountainous areas are often only accessible under leaf-on conditions due to snow cover precluding leaf-off surveys. Regulatory constraints can further restrict the acquisition window in some regions. These operational realities motivate the development of models capable of handling heterogeneous acquisition conditions, precisely the challenge that the full FLORA model addresses.

4.3.4. The full model as a robust operational solution

The full model, trained on both leaf-on and leaf-off data, consistently outperforms season-specific models regardless of the test set phenology. In same-season evaluation, its advantage is clearest on leaf-off, where it reduces total volume rRMSE from 39.67% to 36.21% and nearly halves the height

error gap (11.44% vs. 16.08%, $R^2 = 0.81$ vs. 0.63). In cross-season setting, it avoids the severe degradation of the leaf-off-specific model, maintaining volume rRMSE at 40.83% on leaf-on, where the leaf-off model reaches 65.15%. This is consistent with White et al. (2015), who show that pooled models trained on both seasons achieve intermediate performance between leaf-on and leaf-off models in same-season evaluation, while substantially outperforming cross-season model-mixing. Our results extend this finding to a DL setting at the national scale, suggesting that training on heterogeneous phenological conditions is not only feasible but produces more robust predictions than any season-specific strategy, a practically important result given the uneven and fragmented nature of leaf-on/leaf-off coverage across the French national LiDAR programme.

4.4. Contribution of overlapping acquisitions

Overlapping plots *i.e.*, surveyed under both leaf-on and leaf-off conditions, provide a unique training signal by anchoring the model to paired observations of the same forest under contrasting contexts. The results in Table D.9 and Figure 5 show that exploiting these overlaps yields contrasting effects, depending on the target attribute. Performance improves most clearly for total and deciduous volume, with rRMSE reductions of approximately 5 and 12 points respectively. This suggests that paired phenological observations help the model better disentangle broadleaf structural signals across seasons. Height also shows modest but consistent improvements under the overlap condition. These gains are coherent with the premise that co-registered multi-seasonal acquisitions provide complementary canopy penetration profiles that are informative for broadleaf volume estimation (Ørka et al., 2010; Davison et al., 2020).

Coniferous volume shows the opposite trend, with rRMSE increasing from 73.15% to 80.87% and R^2 dropping from 0.441 to 0.324 under the overlap condition. Basal area and stem density also degrade slightly. This result is counterintuitive but may reflect the limited size and geographic scope of the overlap subset: overlapping areas represent a geographically constrained fraction of the territory, and the model trained on these plots may lack sufficient diversity in coniferous stand types to generalize. Furthermore, coniferous stands are structurally more stable across phenological conditions than deciduous stands (Wasser et al., 2013), meaning that paired leaf-on/leaf-off observations provide comparatively less complementary structural information for conifers. As a result, restricting training to overlap plots likely

reduces effective sample diversity, without providing the compensating benefit of paired phenological contrast that drives improvements for broadleaf volume estimation. This suggests that exploiting dense optical time series (*e.g.*, Landsat or Sentinel-2) can help mitigate these limitations by capturing phenological variability that single-date or acquisition-tied observations cannot resolve. Time series approaches improve the discrimination of forest types by separating phenology-driven spectral signals from structural variability, which is particularly relevant in mixed or conifer-dominated stands where seasonal contrast is weaker and less informative (Guindon et al., 2024).

4.5. Added value of auxiliary variables

The relevance of contextual variables was evaluated both through direct Aux (FLORA)/No Aux comparisons (Appendix A and Appendix C) and through ablation gating analysis (Figure 7). Together, these results reveal that auxiliary metadata provides limited improvements in overall and same-season conditions, but substantial gains in cross-season generalization, with strong contrasts across forest attributes and forest-type strata.

The improvements become much larger in cross-season settings. Both season-specific models exhibit strong error inflation when tested on the opposite season, and in these cases auxiliary metadata plays a major stabilizing role. For example, the leaf-off model tested on leaf-on exhibits rRMSE reductions from 97.7% to 65.1% for total volume, from 121.9% to 85.9% for coniferous volume, and from 367% to 196% for deciduous volume. Similar effects are observed for the leaf-on model cross-tested on leaf-off, with deciduous volume rRMSE improving from 168.8% to 129.4%. These results confirm that temporal and ecological metadata compensate for seasonal structural shifts—especially in leaf-off acquisitions where canopy geometry is less informative.

Coniferous volume and **deciduous volume** benefit the most from auxiliary information, consistent with their low geometric discriminability in the point cloud. Ablation gates identify **delta**, **center** and **SER** as the most influential variables, and the Aux/No Aux comparisons confirm this through systematic rRMSE and R^2 gains for pure coniferous and pure deciduous stands. This is coherent with the strong spatial segregation of species types (*e.g.*, coniferous stands at higher elevation), which the contextual variables make explicit. In contrast, mixed stands often degrade when auxiliary data is added, suggesting that ecological metadata pushes the model towards

over-interpreting coarse species patterns that do not reflect the finer structural mosaics of mixed forests.

Total volume and basal area show moderate gate activations and correspondingly modest but stable improvements, particularly through the **center** and **ser** variables. These two variables capture regional trends in productivity and forest structure that LiDAR alone cannot fully encode. Their effects remain positive across most models and test conditions.

Height is the only attribute essentially unaffected by auxiliary metadata. Gate activations are heterogeneous but do not translate into performance gains/ The Aux/No Aux comparisons across all tables show changes below 0.2% rRMSE. This confirms that height is almost entirely determined by LiDAR canopy geometry and largely independent of ecological descriptors.

Stem density exhibits a more complex pattern. In same-season tests, auxiliary variables mildly degrade performance, consistent with shortcut learning dynamics where categorical metadata encodes coarse density priors that interfere with the structurally weak LiDAR signal. However, in cross-season tests, the effect reverses: density rRMSE improves substantially (*e.g.*, 82.1% → 67.8% for the leaf-off model tested on leaf-on). Thus, while metadata can be detrimental in homogeneous acquisition contexts, it provides valuable stabilization when acquisition conditions shift, mirroring the behaviour observed for species-specific volumes.

Overall, **center**, **ser**, and **delta** stand out as the variables providing the most reliable improvements—particularly for volume-related attributes and in cross-season scenarios—while **date** and **cover** contribute little or inconsistently. The convergence of direct performance comparisons and gating analysis highlights that auxiliary variables are not universally beneficial but become crucial whenever LiDAR geometry alone is insufficient to capture ecological variability or to bridge strong shifts in acquisition conditions.

5. Conclusion

This study introduced **FLORA**, a voxel-based DL framework for predicting six forest structural attributes from heterogeneous airborne LiDAR data at national scale, trained and evaluated on 32,052 NFI plots across mainland France.

The main findings are as follows. A single model trained jointly on leaf-on and leaf-off acquisitions consistently outperforms season-specific models, including within their respective calibration domains, and avoids the strong

cross-season degradation observed when leaf-off models are applied to leaf-on data. The initial class imbalance between leaf-on and leaf-off samples does not bias the full model, and using all available training data proves preferable to enforcing class balance. Plots acquired under both phenological conditions improve estimates of broadleaf and total volume, while their benefit for coniferous stands is limited. Auxiliary contextual variables provide modest but consistent gains, particularly for species-specific volumes and cross-season generalization, whereas dominant height is driven almost entirely by point cloud geometry.

Overall, these results show that a generic DL approach trained on sufficiently large and diverse national-scale data can handle acquisition heterogeneity such as that of the French LiDAR HD without explicit stratification by season, sensor, or forest type. The model also exhibits strong generalization, an increasingly critical requirement for large-scale applications where LiDAR acquisitions are spatially heterogeneous, calling for methods capable of robust performance over extensive areas. Species-specific volume prediction remains the main limitation, highlighting the need to integrate dense optical time series to better capture phenological variation and enable operational wall-to-wall mapping.

6. CRediT authorship contribution statement

Emilie Vautier: Writing – original draft, Writing – review and editing, Data Curation, Conceptualization, Investigation, Methodology, Formal Analysis, Software, Validation, Visualization

Clément Mallet: Writing – review and editing, Conceptualization, Methodology, Formal Analysis, Supervision

Cédric Vega: Writing – review and editing, Conceptualization, Methodology, Formal Analysis, Supervision

7. Declaration of Competing Interest

The authors declare that there are no conflicts of interest associated with this work.

Appendix A. Detailed results of FLORA trained on the full training set

Metric / Species		leaf-on testing				leaf-off testing			
		No Aux		FLORA		No Aux		FLORA	
		rRMSE	R ²	rRMSE	R ²	rRMSE	R ²	rRMSE	R ²
Full model									
Volume	All	41.56	0.75	40.83↑	0.76 ↑	36.23	0.67	36.21 ↑	0.67 ↑
	Coniferous	42.66	0.64	40.23↑	0.68 ↑	37.21	0.62	36.84 ↑	0.63 ↑
	Deciduous	40.24	0.81	37.95↑	0.83 ↑	30.95	0.68	30.23 ↑	0.70 ↑
	Mixed	38.85	0.73	44.88↓	0.64 ↓	36.71	0.69	39.94↓	0.64 ↓
Conif. Vol.	All	55.96	0.73	53.95↑	0.75 ↑	42.87	0.69	43.09↓	0.69 ↓
	Coniferous	43.77	0.63	41.77↑	0.67 ↑	38.72	0.61	38.26 ↑	0.62 ↑
	Deciduous	324.43	-0.33	262.18↑	0.13 ↑	245.65	-1.16	218.87 ↑	-0.71 ↑
	Mixed	78.69	0.44	83.36↓	0.37 ↓	58.57	0.47	75.84↓	0.11 ↓
Decid. Vol.	All	77.11	0.82	77.23↓	0.82 ↓	96.11	0.83	96.25↓	0.83 ↓
	Coniferous	500.27	-1.20	469.37 ↑	-0.93 ↑	632.95	-1.23	562.25↑	-0.76 ↑
	Deciduous	43.08	0.79	40.55↑	0.81 ↑	35.56	0.61	35.42 ↑	0.61 ↑
	Mixed	62.03	0.51	71.31↓	0.35 ↓	59.48	0.55	64.78↓	0.47 ↓
Density	All	54.86	0.44	53.72 ↑	0.47 ↑	55.34	0.46	57.44↓	0.42 ↓
	Coniferous	56.08	0.43	54.77 ↑	0.45 ↑	55.25	0.47	56.93↓	0.43 ↓
	Deciduous	49.97	0.47	49.77 ↑	0.47 ↑	57.97	0.44	59.54↓	0.41 ↓
	Mixed	50.89	0.33	49.69 ↑	0.36 ↑	52.23	0.43	58.24↓	0.29 ↓
Basal Area	All	38.02	0.53	36.81↑	0.56 ↑	33.47	0.49	34.03↓	0.48 ↓
	Coniferous	39.74	0.41	37.87↑	0.46 ↑	34.71	0.45	34.39 ↑	0.46 ↑
	Deciduous	35.42	0.66	33.49↑	0.69 ↑	27.71	0.43	29.68↓	0.35 ↓
	Mixed	36.80	0.55	38.69↓	0.51 ↓	33.04	0.57	37.12↓	0.46 ↓
Height	All	12.65	0.90	12.81↓	0.89 ↓	11.23	0.82	11.44↓	0.81 ↓
	Coniferous	13.00	0.88	12.83↑	0.89 ↑	11.35	0.80	11.67↓	0.79 ↓
	Deciduous	12.39	0.92	12.79↓	0.91 ↓	10.28	0.87	10.30↓	0.87 ↓
	Mixed	11.78	0.90	12.78↓	0.88 ↓	11.49	0.83	10.98 ↑	0.85 ↑

Table A.4: The full model, trained on both leaf-off and leaf-on samples, is evaluated on leaf-on and leaf-off test sets. Performance is reported in terms of rRMSE and R² for both FLORA and No Aux configurations. Arrows on FLORA values indicate whether FLORA outperforms No Aux (↑ FLORA better, ↓ No Aux better).

Appendix B. Detailed results of FLORA comparing balanced and non-balanced full training sets

Metric / Species		Same-season testing				Cross-season testing			
		No Aux		FLORA		No Aux		FLORA	
		rRMSE	R ²	rRMSE	R ²	rRMSE	R ²	rRMSE	R ²
leaf-on model									
Volume	All	43.22	0.73	45.19↓	0.70 ↓	41.27	0.57	40.87↑	0.57 ↑
	Coniferous	43.99	0.62	45.67↓	0.59 ↓	42.07	0.52	42.72↓	0.50 ↓
	Deciduous	40.78	0.80	42.17↓	0.79 ↓	35.88	0.57	31.66↑	0.67 ↑
	Mixed	43.47	0.66	47.01↓	0.60 ↓	42.60	0.59	42.44↑	0.59 ↑
Conif. Vol.	All	59.92	0.69	64.03↓	0.65 ↓	55.26	0.49	52.51↑	0.54 ↑
	Coniferous	45.50	0.60	48.60↓	0.55 ↓	50.12	0.34	47.46↑	0.41 ↑
	Deciduous	428.52	-1.31	412.17↑	-1.14 ↑	258.49	-1.39	239.04↑	1.04 ↑
	Mixed	90.01	0.26	100.18↓	0.09 ↓	77.55	0.07	78.16↓	0.05 ↓
Decid. Vol.	All	80.39	0.80	87.91↓	0.76 ↓	147.93	0.59	132.61↑	0.67 ↑
	Coniferous	451.91	-0.79	542.15↓	-1.58 ↓	1598.73	-13.22	1248.58↑	-7.67 ↑
	Deciduous	45.06	0.77	47.38↓	0.74 ↓	39.89	0.51	42.04↓	0.45 ↓
	Mixed	68.64	0.40	77.52↓	0.24 ↓	70.85	0.36	69.10↑	0.40 ↑
Density	All	58.92	0.36	57.92↑	0.38 ↑	65.17	0.25	67.15↓	0.20 ↓
	Coniferous	60.70	0.33	58.92↑	0.37 ↑	65.30	0.25	66.90↓	0.22 ↓
	Deciduous	53.65	0.39	54.68↓	0.37 ↓	65.66	0.28	70.00↓	0.18 ↓
	Mixed	52.01	0.30	52.95↓	0.28 ↓	63.32	0.16	65.06↓	0.11 ↓
Basal Area	All	39.48	0.50	40.38↓	0.47 ↓	38.31	0.34	41.06↓	0.24 ↓
	Coniferous	41.14	0.37	41.77↓	0.35 ↓	39.74	0.28	42.60↓	0.17 ↓
	Deciduous	36.23	0.64	36.69↓	0.63 ↓	31.41	0.27	33.52↓	0.17 ↓
	Mixed	39.48	0.49	41.88↓	0.42 ↓	38.24	0.42	41.09↓	0.33 ↓
Height	All	15.87	0.84	14.97↑	0.86 ↑	12.63	0.77	12.40↑	0.78 ↑
	Coniferous	16.31	0.82	15.00↑	0.85 ↑	12.78	0.75	12.73↑	0.75 ↑
	Deciduous	15.43	0.87	15.66↓	0.87 ↓	12.45	0.82	11.24↑	0.85 ↑
	Mixed	15.02	0.84	13.71↑	0.86 ↑	11.55	0.83	10.97↑	0.85 ↑

Table B.5: The leaf-on model, trained exclusively on leaf-on samples, is evaluated on a same-season test set (leaf-on) and cross-tested on the leaf-off season. Performance is reported in rRMSE and R² for both FLORA (with auxiliary data) and No Aux configurations. Arrows on FLORA values indicate whether FLORA outperforms No Aux (↑ FLORA better, ↓ No Aux better).

Metric / Species		leaf-on testing				leaf-off testing			
		No Aux		FLORA		No Aux		FLORA	
		rRMSE	R ²	rRMSE	R ²	rRMSE	R ²	rRMSE	R ²
Full model									
Volume	All	43.23	0.73	43.27↓	0.73 ↓	38.61	0.62	36.09↑	0.67 ↑
	Coniferous	43.67	0.62	43.05↑	0.63 ↑	39.29	0.58	37.56↑	0.62 ↑
	Deciduous	41.24	0.80	42.37↓	0.79 ↓	36.31	0.56	26.51↑	0.77 ↑
	Mixed	43.34	0.66	42.69↑	0.67 ↑	34.89	0.72	40.51↓	0.63 ↓
Conif. Vol.	All	57.34	0.72	59.96↓	0.69 ↓	44.78	0.66	45.35↓	0.66 ↓
	Coniferous	44.72	0.62	46.78↓	0.58 ↓	40.29	0.58	40.23↑	0.58 ↑
	Deciduous	347.55	-0.52	283.88↑	-0.01 ↑	223.65	-0.79	215.46↑	-0.66 ↑
	Mixed	80.70	0.41	89.86↓	0.27 ↓	68.73	0.27	81.95↓	-0.04 ↓
Decid. Vol.	All	78.77	0.81	81.86↓	0.79 ↓	106.02	0.79	96.75↑	0.83 ↑
	Coniferous	534.99	-1.51	604.75↓	-2.21 ↓	677.63	-1.55	833.62↓	-2.87 ↓
	Deciduous	42.48	0.79	43.70↓	0.78 ↓	40.36	0.49	28.62↑	0.75 ↑
	Mixed	66.18	0.44	66.40↓	0.44 ↓	63.42	0.49	63.98↓	0.48 ↓
Density	All	56.78	0.40	56.46↑	0.41 ↑	58.19	0.40	56.90↑	0.43 ↑
	Coniferous	58.06	0.39	57.63↑	0.40 ↑	57.71	0.42	55.98↑	0.45 ↑
	Deciduous	52.11	0.42	51.69↑	0.43 ↑	62.00	0.36	61.05↑	0.38 ↑
	Mixed	52.13	0.30	52.51↓	0.29 ↓	56.42	0.33	57.90↓	0.30 ↓
Basal Area	All	38.94	0.51	37.74↑	0.54 ↑	35.55	0.43	33.87↑	0.48 ↑
	Coniferous	40.68	0.38	38.84↑	0.43 ↑	37.03	0.38	34.76↑	0.45 ↑
	Deciduous	35.61	0.65	34.73↑	0.67 ↑	31.81	0.25	26.51↑	0.48 ↑
	Mixed	38.83	0.50	39.03↓	0.50 ↓	29.75	0.65	37.94↓	0.43 ↓
Height	All	13.18	0.89	13.69↓	0.88 ↓	11.82	0.80	11.35↑	0.81 ↑
	Coniferous	13.69	0.87	14.00↓	0.87 ↓	11.76	0.79	11.60↑	0.79 ↑
	Deciduous	12.61	0.92	13.62↓	0.90 ↓	11.34	0.85	9.55↑	0.89 ↑
	Mixed	12.22	0.89	12.67↓	0.88 ↓	12.90	0.79	11.49↑	0.83 ↑

Table B.6: The full model, trained on both leaf-off and leaf-on samples, is evaluated on leaf-on and leaf-off test sets. Performance is reported in terms of rRMSE and R² for both FLORA (with auxiliary data) and No Aux configurations. Arrows on FLORA values indicate whether FLORA outperforms No Aux (↑ FLORA better, ↓ No Aux better).

Appendix C. Results for season-specific model

Metric / Species		Same-season testing				Cross-season testing			
		No Aux		FLORA		No Aux		FLORA	
		rRMSE	R ²	rRMSE	R ²	rRMSE	R ²	rRMSE	R ²
leaf-on model									
Volume	All	42.07	0.74	41.80↑	0.75 ↑	39.96	0.59	39.43 ↑	0.60 ↑
	Coniferous	40.99	0.67	41.65↓	0.66 ↓	40.48	0.55	40.97↓	0.54 ↓
	Deciduous	42.29	0.79	40.33↑	0.81 ↑	35.87	0.57	29.76 ↑	0.71 ↑
	Mixed	41.16	0.70	42.31↓	0.68 ↓	40.76	0.62	43.49↓	0.57 ↓
Conif. Vol.	All	57.19	0.72	57.49↓	0.72 ↓	51.89	0.55	50.33 ↑	0.58 ↑
	Coniferous	43.21	0.64	43.81↓	0.63 ↓	46.93	0.42	45.30↑	0.46 ↑
	Deciduous	440.39	-1.44	347.81↑	-0.52 ↑	309.63	-2.43	257.96 ↑	-1.38 ↑
	Mixed	84.88	0.35	90.22↓	0.26 ↓	67.63	0.29	76.23↓	0.10 ↓
Decid. Vol.	All	82.01	0.79	84.10↓	0.78 ↓	168.83	0.47	129.40↑	0.69 ↑
	Coniferous	428.56	-0.61	601.76↓	-2.18 ↓	1909.48	-19.28	1216.73↑	-7.23 ↑
	Deciduous	48.03	0.73	45.33↑	0.76 ↑	43.68	0.41	38.01 ↑	0.55 ↑
	Mixed	65.56	0.45	68.48↓	0.40 ↓	72.67	0.33	76.38↓	0.26 ↓
Density	All	55.93	0.42	54.15 ↑	0.46 ↑	73.63	0.04	63.37↑	0.29 ↑
	Coniferous	56.13	0.43	54.47 ↑	0.46 ↑	76.54	-0.02	63.38↑	0.30 ↑
	Deciduous	55.65	0.34	50.86 ↑	0.45 ↑	63.89	0.32	66.21↓	0.27 ↓
	Mixed	51.74	0.31	53.18↓	0.27 ↓	62.54	0.18	59.21↑	0.26 ↑
Basal Area	All	38.01	0.53	37.79↑	0.54 ↑	38.66	0.32	37.77 ↑	0.36 ↑
	Coniferous	39.29	0.42	38.79 ↑	0.44 ↑	40.62	0.25	39.33↑	0.30 ↑
	Deciduous	35.95	0.65	34.46↑	0.68 ↑	29.92	0.34	29.79 ↑	0.35 ↑
	Mixed	37.27	0.54	39.87↓	0.48 ↓	37.69	0.44	38.43↓	0.42 ↓
Height	All	13.77	0.88	13.98↓	0.87 ↓	12.45	0.78	12.22 ↑	0.78 ↑
	Coniferous	13.39	0.88	14.24↓	0.86 ↓	12.86	0.75	12.64 ↑	0.76 ↑
	Deciduous	14.77	0.88	14.00↑	0.90 ↑	11.04	0.86	10.28 ↑	0.88 ↑
	Mixed	13.37	0.87	12.97↑	0.88 ↑	10.55	0.86	11.04↓	0.85 ↓

Table C.7: The leaf-on model, trained exclusively on leaf-on samples, is evaluated on a same-season test set (leaf-on) and cross-tested on the leaf-off season. Performance is reported in rRMSE and R² for both FLORA (with auxiliary data) and No Aux configurations. Arrows on FLORA values indicate whether FLORA outperforms No Aux (↑ FLORA better, ↓ No Aux better).

Metric / Species		Same-season testing				Cross-season testing			
		No Aux		FLORA		No Aux		FLORA	
		rRMSE	R ²	rRMSE	R ²	rRMSE	R ²	rRMSE	R ²
leaf-off model									
Volume	All	39.71	0.60	39.67 ↑	0.60 ↑	97.72	-0.39	65.15↑	0.38 ↑
	Coniferous	39.42	0.58	40.50↓	0.55 ↓	130.64	-2.38	77.59↑	-0.19 ↑
	Deciduous	38.89	0.50	35.20 ↑	0.59 ↑	48.70	0.72	48.24↑	0.72 ↑
	Mixed	38.90	0.66	39.31↓	0.65 ↓	78.19	-0.10	60.17↑	0.35 ↑
Conif. Vol.	All	50.58	0.57	54.03↓	0.51 ↓	121.90	-0.27	85.96↑	0.37 ↑
	Coniferous	45.35	0.46	47.82↓	0.40 ↓	97.37	-0.81	65.49↑	0.18 ↑
	Deciduous	298.93	-2.20	309.02↓	-2.42 ↓	645.37	-4.24	488.87↑	-2.01 ↑
	Mixed	75.72	0.11	94.50↓	-0.38 ↓	155.52	-1.20	137.30↑	-0.71 ↑
Decid. Vol.	All	150.25	0.58	118.77 ↑	0.74 ↑	367.27	-3.16	196.29↑	-0.19 ↑
	Coniferous	974.51	-4.28	1009.99↓	-4.67 ↓	5389.02	253.74	2512.15↑	-54.36 ↑
	Deciduous	58.61	-0.07	40.20 ↑	0.50 ↑	73.36	0.38	53.58↑	0.67 ↑
	Mixed	83.81	0.11	65.77 ↑	0.45 ↑	215.28	-4.90	156.83↑	-2.13 ↑
Density	All	59.55	0.37	58.67 ↑	0.39 ↑	82.15	-0.25	67.79↑	0.15 ↑
	Coniferous	59.25	0.39	57.98 ↑	0.41 ↑	83.54	-0.27	70.93↑	0.08 ↑
	Deciduous	65.56	0.28	63.31↑	0.33 ↑	75.13	-0.20	55.94 ↑	0.34 ↑
	Mixed	53.01	0.41	57.37↓	0.31 ↓	78.28	-0.58	60.27↑	0.07 ↑
Basal Area	All	36.46	0.40	35.79 ↑	0.42 ↑	74.78	-0.80	53.50↑	0.08 ↑
	Coniferous	36.97	0.38	36.88 ↑	0.38 ↑	92.07	-2.18	61.96↑	-0.44 ↑
	Deciduous	34.93	0.10	30.17 ↑	0.33 ↑	42.26	0.51	39.47↑	0.58 ↑
	Mixed	33.81	0.55	36.12↓	0.49 ↓	61.02	-0.22	47.24↑	0.27 ↑
Height	All	16.48	0.61	16.08 ↑	0.63 ↑	17.45	0.80	18.60↓	0.78 ↓
	Coniferous	16.83	0.57	16.15 ↑	0.60 ↑	17.41	0.79	19.20↓	0.75 ↓
	Deciduous	14.27	0.76	16.10↓	0.69 ↓	18.13	0.82	18.15↓	0.82 ↓
	Mixed	16.35	0.66	15.38 ↑	0.70 ↑	16.44	0.80	17.14↓	0.79 ↓

Table C.8: The leaf-off model, trained exclusively on leaf-off samples, is evaluated on a same-season test set (leaf-off) and cross-tested on the leaf-on season. Performance is reported in rRMSE and R² for both FLORA (with auxiliary data) and No Aux configurations. Arrows on FLORA values indicate whether FLORA outperforms No Aux (↑ FLORA better, ↓ No Aux better).

Appendix D. Overlapping acquisitions

Metric / Species		With overlaps		Without overlaps	
		rRMSE	R ²	rRMSE	R ²
Volume	All	52.94	0.499	58.26 ± 1.45	0.420 ± 0.029
	Coniferous	52.01	0.412	54.02 ± 3.47	0.350 ± 0.084
	Deciduous	52.14	0.576	63.89 ± 4.98	0.431 ± 0.087
	Mixed	54.68	0.457	54.44 ± 3.56	0.439 ± 0.074
Conif. Vol.	All	80.87	0.324	73.15 ± 1.04	0.441 ± 0.016
	Coniferous	55.72	0.344	54.63 ± 1.41	0.364 ± 0.033
	Deciduous	1308.53	-23.456	874.49 ± 147.66	-11.434 ± 3.925
	Mixed	111.06	-0.164	113.14 ± 2.75	-0.304 ± 0.063
Decid. Vol.	All	135.11	0.496	147.33 ± 4.68	0.421 ± 0.037
	Coniferous	880.14	-4.212	827.85 ± 297.72	-4.809 ± 4.054
	Deciduous	68.68	0.292	80.15 ± 9.12	0.130 ± 0.195
	Mixed	100.36	-0.107	97.16 ± 1.55	-0.200 ± 0.039
Density	All	74.58	0.033	72.88 ± 1.68	0.044 ± 0.044
	Coniferous	72.94	0.116	73.00 ± 3.06	0.085 ± 0.078
	Deciduous	79.80	-0.358	76.32 ± 3.20	-0.170 ± 0.097
	Mixed	74.71	-0.184	65.50 ± 1.25	-0.055 ± 0.040
Basal Area	All	51.58	0.059	47.34 ± 1.19	0.212 ± 0.039
	Coniferous	52.73	-0.085	47.14 ± 1.93	0.111 ± 0.073
	Deciduous	49.77	0.195	47.64 ± 5.22	0.285 ± 0.159
	Mixed	49.45	0.140	46.03 ± 0.73	0.281 ± 0.023
Height	All	19.89	0.702	20.75 ± 1.07	0.669 ± 0.035
	Coniferous	19.58	0.688	20.25 ± 0.84	0.652 ± 0.029
	Deciduous	20.70	0.738	23.02 ± 1.56	0.690 ± 0.043
	Mixed	20.05	0.693	19.38 ± 1.52	0.701 ± 0.047

Table D.9: Effect of spatial overlap between acquisitions on full model performance. Metrics are reported as rRMSE and R² for models trained with auxiliary data (FLORA). Results on non-overlapping areas correspond to mean ± std over K runs.

Appendix E. Auxiliary data

Metric / Species		No Meta (Ref)		Comp.		Cover		SER	
		rRMSE	R ²	rRMSE	R ²	rRMSE	R ²	rRMSE	R ²
Volume	All	39.78	0.7297	+0.00↓	+0.0001↑	-0.34↑	+0.0046↑	-0.59↑	+0.0080↑
	Coniferous	40.37	0.6384	-0.52↑	+0.0093↑	-0.68↑	+0.0121↑	-1.07↑	+0.0190↑
	Deciduous	38.30	0.7966	-0.01↑	+0.0002↑	-0.55↑	+0.0058↑	-1.16↑	+0.0122↑
	Mixed	38.36	0.7226	+1.68↓	-0.0249↓	+1.20↓	-0.0176↓	+2.10↓	-0.0313↓
Conif. Vol.	All	50.73	0.7311	-0.43↑	+0.0046↑	-0.87↑	+0.0092↑	-1.25↑	+0.0131↑
	Coniferous	41.64	0.6307	-0.58↑	+0.0102↑	-0.87↑	+0.0151↑	-1.14↑	+0.0199↑
	Deciduous	305.45	-0.4749	-41.31↑	+0.3720↑	-12.58↑	+0.1190↑	-17.78↑	+0.1667↑
	Mixed	73.57	0.4490	+5.31↓	-0.0825↓	+1.30↓	-0.0196↓	+0.53↓	-0.0079↓
Decid. Vol.	All	81.86	0.8213	-4.71↑	+0.0199↑	-3.33↑	+0.0142↑	-5.16↑	+0.0218↑
	Coniferous	540.66	-1.1938	-151.64↑	+1.0580↑	-22.19↑	+0.1764↑	-111.67↑	+0.8127↑
	Deciduous	41.53	0.7695	-1.20↑	+0.0131↑	-1.30↑	+0.0141↑	-1.83↑	+0.0199↑
	Mixed	61.50	0.5193	-0.05↑	+0.0008↑	-3.72↑	+0.0563↑	-1.47↑	+0.0226↑
Density	All	55.15	0.4530	+0.26↓	-0.0051↓	+0.27↓	-0.0054↓	+0.50↓	-0.0100↓
	Coniferous	56.38	0.4553	-0.29↑	+0.0056↑	-0.65↑	+0.0123↑	+0.87↓	-0.0169↓
	Deciduous	51.69	0.4644	+1.74↓	-0.0366↓	+2.09↓	-0.0441↓	-0.70↑	+0.0145↑
	Mixed	51.17	0.3565	+1.63↓	-0.0415↓	+3.27↓	-0.0848↓	-0.21↑	+0.0053↑
Basal Area	All	36.76	0.5255	-0.22↑	+0.0057↑	-0.37↑	+0.0095↑	-0.87↑	+0.0223↑
	Coniferous	38.01	0.4228	-0.50↑	+0.0153↑	-0.38↑	+0.0116↑	-0.92↑	+0.0278↑
	Deciduous	33.99	0.6402	-0.25↑	+0.0052↑	-0.83↑	+0.0173↑	-1.79↑	+0.0369↑
	Mixed	36.09	0.5579	+0.87↓	-0.0216↓	+0.42↓	-0.0104↓	+0.79↓	-0.0198↓
Height	All	12.16	0.8869	-0.41↑	+0.0074↑	+0.04↓	-0.0009↓	-0.47↑	+0.0084↑
	Coniferous	12.30	0.8718	-0.20↑	+0.0043↑	+0.24↓	-0.0049↓	-0.35↑	+0.0074↑
	Deciduous	11.96	0.9166	-1.11↑	+0.0147↑	-0.44↑	+0.0061↑	-1.04↑	+0.0138↑
	Mixed	11.73	0.8912	-0.36↑	+0.0064↑	-0.16↑	+0.0029↑	-0.13↑	+0.0023↑

Table E.10: Ecological auxiliary variables (composition, cover, SER).

Metric / Species		No Meta (Ref)		Center		Date		Delta	
		rRMSE	R ²	rRMSE	R ²	rRMSE	R ²	rRMSE	R ²
Volume	All	39.78	0.7297	-1.45↑	+0.0194↑	+0.45↓	-0.0061↓	-0.09↑	+0.0012↑
	Coniferous	40.37	0.6384	-1.20↑	+0.0212↑	-0.39↑	+0.0070↑	-0.27↑	+0.0048↑
	Deciduous	38.30	0.7966	-3.34↑	+0.0339↑	+0.48↓	-0.0051↓	-0.31↑	+0.0033↑
	Mixed	38.36	0.7226	+1.42↓	-0.0210↓	+3.02↓	-0.0454↓	+0.94↓	-0.0138↓
Conif. Vol.	All	50.73	0.7311	-1.99↑	+0.0207↑	-0.30↑	+0.0032↑	-0.77↑	+0.0081↑
	Coniferous	41.64	0.6307	-1.96↑	+0.0340↑	-0.81↑	+0.0141↑	-0.37↑	+0.0064↑
	Deciduous	305.45	-0.4749	+4.95↓	-0.0482↓	+30.59↓	-0.3102↓	-35.79↑	+0.3254↑
	Mixed	73.57	0.4490	-0.17↑	+0.0026↑	+3.67↓	-0.0564↓	-2.03↑	+0.0299↑
Decid. Vol.	All	81.86	0.8213	-5.49↑	+0.0231↑	-0.20↑	+0.0009↑	-5.73↑	+0.0241↑
	Coniferous	540.66	-1.1938	-40.13↑	+0.3136↑	-151.45↑	+1.0569↑	-99.42↑	+0.7327↑
	Deciduous	41.53	0.7695	-4.25↑	+0.0447↑	+1.97↓	-0.0225↓	-1.40↑	+0.0152↑
	Mixed	61.50	0.5193	+0.38↓	-0.0061↓	+2.11↓	-0.0336↓	-5.10↑	+0.0764↑
Density	All	55.15	0.4530	+1.35↓	-0.0271↓	-0.16↑	+0.0031↑	+0.55↓	-0.0111↓
	Coniferous	56.38	0.4553	+0.97↓	-0.0191↓	-0.37↑	+0.0070↑	+0.16↓	-0.0031↓
	Deciduous	51.69	0.4644	+1.41↓	-0.0296↓	+0.67↓	-0.0139↓	+0.47↓	-0.0097↓
	Mixed	51.17	0.3565	+3.41↓	-0.0885↓	+0.02↓	-0.0005↓	+2.94↓	-0.0760↓
Basal Area	All	36.76	0.5255	-1.22↑	+0.0310↑	+0.19↓	-0.0050↓	-0.06↑	+0.0014↑
	Coniferous	38.01	0.4228	-1.11↑	+0.0334↑	-0.32↑	+0.0098↑	-0.14↑	+0.0044↑
	Deciduous	33.99	0.6402	-2.55↑	+0.0519↑	+0.72↓	-0.0154↓	-0.50↑	+0.0105↑
	Mixed	36.09	0.5579	+0.51↓	-0.0126↓	+1.24↓	-0.0311↓	+0.99↓	-0.0248↓
Height	All	12.16	0.8869	-0.08↑	+0.0013↑	-0.23↑	+0.0041↑	-0.32↑	+0.0058↑
	Coniferous	12.30	0.8718	+0.08↓	-0.0017↓	-0.04↑	+0.0010↑	-0.19↑	+0.0040↑
	Deciduous	11.96	0.9166	-0.59↑	+0.0079↑	-0.71↑	+0.0096↑	-0.87↑	+0.0117↑
	Mixed	11.73	0.8912	-0.07↑	+0.0012↑	-0.37↑	+0.0067↑	-0.12↑	+0.0021↑

Table E.11: Spatiotemporal auxiliary variables (center, date, delta effects).

References

- Akiba, T., Shotaro, S., Toshihiko, Y., Takeru, O., Masanori, K., 2019. Op-tuna: A next-generation hyperparameter optimization framework. URL: <https://dl.acm.org/doi/epdf/10.1145/3292500.3330701>, doi:10.1145/3292500.3330701.
- Ayrey, E., Hayes, D.J., Kilbride, J.B., Fraver, S., John A. Kershaw, J., Cook, B.D., Weiskittel, A.R., 2021. Synthesizing disparate LiDAR and satellite datasets through deep learning to generate wall-to-wall regional inventories for the complex, mixed-species forests of the eastern United States. Remote Sensing 13. URL: <https://www.mdpi.com/2072-4292/13/24/5113>, doi:10.3390/rs13245113. publisher: Multidisciplinary Digital Publishing Institute.

- Bergstra, J., Bardenet, R., Bengio, Y., Kégl, B., 2011. Algorithms for hyperparameter optimization, in: Shawe-Taylor, J., Zemel, R., Bartlett, P., Pereira, F., Weinberger, K.Q. (Eds.), *Advances in Neural Information Processing Systems*, Curran Associates, Inc.
- Björnberg, D., Ericsson, M., Lindeberg, J., Löwe, W., Nordqvist, J., Wallerman, J., Fransson, J.E., 2026. Improving national forest attribute maps of Sweden with machine learning. *Science of Remote Sensing* 13, 100395. URL: <https://linkinghub.elsevier.com/retrieve/pii/S2666017226000337>, doi:10.1016/j.srs.2026.100395.
- Bontemps, J.D., Hervé, J.C., Denardou, A., 2019. Partition idéalisée et régionalisée de la composition en espèces ligneuses des forêts françaises. *Écoscience* 26, 291–308. URL: <https://doi.org/10.1080/11956860.2019.1588511>, doi:10.1080/11956860.2019.1588511. publisher: Taylor & Francis _eprint: <https://doi.org/10.1080/11956860.2019.1588511>.
- Bornand, A., Abegg, M., Morsdorf, F., Rehus, N., 2024. Completing 3D point clouds of individual trees using deep learning. *Methods in Ecology and Evolution* 15, 2010–2023. URL: <https://besjournals.onlinelibrary.wiley.com/doi/10.1111/2041-210X.14412>, doi:10.1111/2041-210X.14412.
- Borsah, A.A., Nazeer, M., Wong, M.S., 2023. LIDAR-based forest biomass remote sensing: a review of metrics, methods, and assessment criteria for the selection of allometric equations. *Forests* 14. doi:10.3390/f14102095.
- Breidenbach, J., Antón-Fernández, C., Petersson, H., McRoberts, R.E., Astrup, R., 2014. Quantifying the model-related variability of biomass stock and change estimates in the Norwegian national forest inventory. *Forest Science* 60, 25–33. URL: <https://doi.org/10.5849/forsci.12-137>, doi:10.5849/forsci.12-137.
- Coops, N., Tompalski, P., Goodbody, T., Queinnec, M., Luther, J., Bolton, D., White, J., Wulder, M., Lier, O., Hermosilla, T., 2021. Modelling lidar-derived estimates of forest attributes over space and time: A review of approaches and future trends. *Remote Sensing of Environment* 260, 112477. doi:10.1016/j.rse.2021.112477.

- Davison, S., Donoghue, D.N.M., Galiatsatos, N., 2020. The effect of leaf-on and leaf-off forest canopy conditions on LiDAR derived estimations of forest structural diversity. *International Journal of Applied Earth Observation and Geoinformation* 92, 102160. URL: <https://www.sciencedirect.com/science/article/pii/S0303243420300684>, doi:10.1016/j.jag.2020.102160.
- Fan, W., Knoke, T., Troles, J., Tian, J., 2026. Automatic tree-level based forest inventories retrieval via ultra-high resolution UAV images and deep learning. *ISPRS Journal of Photogrammetry and Remote Sensing* 234, 261–274. URL: <https://linkinghub.elsevier.com/retrieve/pii/S0924271626000882>, doi:10.1016/j.isprsjprs.2026.02.029.
- Fareed, N., Silva, C.A., Numata, I., Flores, J.P., 2026. Interdisciplinary applications of LiDAR in forest studies: advances in sensors, methods, and cross-domain metrics. *Remote Sensing* 18. doi:10.3390/rs18020219.
- Gaydon, C., 2022. Myria3D: deep learning for the semantic segmentation of aerial Lidar point clouds. URL: <https://github.com/IGNF/myria3d>. original-date: 2022-01-10T09:50:28Z.
- Gaydon, C., Roche, F., 2025. PureForest: A large-scale aerial Lidar and aerial imagery dataset for tree species classification in monospecific forests, in: *Proceedings of the Winter Conference on Applications of Computer Vision (WACV)*, pp. 5895–5904.
- Geist, L., Landrieu, L., Robert, D., 2025. EZ-SP: fast and lightweight superpoint-based 3D segmentation. URL: <http://arxiv.org/abs/2512.00385>, doi:10.48550/arXiv.2512.00385. arXiv:2512.00385 [cs].
- Gopalakrishnan, R., Thomas, V.A., Coulston, J.W., Wynne, R.H., 2015. Prediction of canopy heights over a large region using heterogeneous Lidar datasets: efficacy and challenges. *Remote Sensing* doi:10.3390/rs70911036.
- Guindon, L., Manka, F., Correia, D.L., Villemaire, P., Smiley, B., Bernier, P., Gauthier, S., Beaudoin, A., Boucher, J., Boulanger, Y., 2024. A new approach for spatializing the Canadian National Forest Inventory (SCANFI) using Landsat dense time series. *Canadian Journal of Forest Research* 54,

- 793–815. URL: <https://cdnsiencepub.com/doi/10.1139/cjfr-2023-0118>, doi:10.1139/cjfr-2023-0118.
- Hauglin, M., Rahlf, J., Schumacher, J., Astrup, R., Breidenbach, J., 2021. Large scale mapping of forest attributes using heterogeneous sets of airborne laser scanning and National Forest Inventory data. *Forest Ecosystems* 8, 65. URL: <https://www.sciencedirect.com/science/article/pii/S2197562023000374>, doi:10.1186/s40663-021-00338-4.
- Hawryło, P., Francini, S., Chirici, G., Giannetti, F., Parkitna, K., Krok, G., Mitelsztedt, K., Lisańczuk, M., Stereńczak, K., Ciesielski, M., Weżyk, P., Socha, J., 2020. The use of remotely sensed data and Polish NFI plots for prediction of growing stock volume using different predictive methods. *Remote Sensing* 12, 3331. URL: <https://www.mdpi.com/2072-4292/12/20/3331>, doi:10.3390/rs12203331.
- IGN, 2025. Mémento inventaire forestier IGN - 2025. URL: <https://www.calameo.com/read/0011885827c418636cbd4>.
- Irulappa-Pillai-Vijayakumar, D.B., Renaud, J.P., Morneau, F., McRoberts, R.E., Vega, C., 2019. Increasing precision for french forest inventory estimates using the k-NN technique with optical and photogrammetric data and model-assisted estimators. *Remote Sensing* 11. URL: <https://www.mdpi.com/2072-4292/11/8/991>, doi:10.3390/rs11080991. publisher: Multidisciplinary Digital Publishing Institute.
- Jakubowski, M.K., Guo, Q., Kelly, M., 2013. Tradeoffs between lidar pulse density and forest measurement accuracy. *Remote Sensing of Environment* 130, 245–253. URL: <https://linkinghub.elsevier.com/retrieve/pii/S0034425712004567>, doi:10.1016/j.rse.2012.11.024.
- Japkowicz, N., Stephen, S., 2002. The class imbalance problem: A systematic study1. *Intelligent Data Analysis* 6, 429–449. URL: <https://journals.sagepub.com/action/showAbstract>, doi:10.3233/IDA-2002-6504. publisher: SAGE Publications.
- Kalinicheva, E., Helen, F., Mermoz, S., Mouret, F., Planells, M., 2025. Super-resolved canopy height mapping from Sentinel-2 time series using LiDAR HD reference data across metropolitan France. doi:10.48550/arXiv.2512.11524. arXiv:2512.11524.

- Karakutuk, A.K., Ozdemir, O., Senturk, S., Karakutuk, A.K., Ozdemir, O., Senturk, S., 2025. Optuna-optimized pythagorean fuzzy deep neural network: a novel framework for uncertainty-aware image classification. *Applied Sciences* 15. doi:10.3390/app152011097.
- Keskar, N.S., Mudigere, D., Nocedal, J., Smelyanskiy, M., Tang, P.T.P., 2017. On large-batch training for deep learning: generalization gap and sharp minima. URL: <http://arxiv.org/abs/1609.04836>, doi:10.48550/arXiv.1609.04836. arXiv:1609.04836 [cs.LG].
- Keskes, M.I., Mohamed, A.H., Borz, S.A., Niță, M.D., 2025. Improving national forest mapping in Romania using machine learning and Sentinel-2 multispectral imagery. *Remote Sensing* 17, 715. URL: <https://www.mdpi.com/2072-4292/17/4/715>, doi:10.3390/rs17040715.
- LaRue, E.A., Fahey, R., Fuson, T.L., Foster, J.R., Matthes, J.H., Krause, K., Hardiman, B.S., 2022. Evaluating the sensitivity of forest structural diversity characterization to LiDAR point density. *Ecosphere* 13, e4209. URL: <https://esajournals.onlinelibrary.wiley.com/doi/10.1002/ecs2.4209>, doi:10.1002/ecs2.4209.
- Leonardo, E.M.C., Watt, M.S., Pearse, G.D., Dash, J.P., Persson, H.J., 2020. Comparison of TanDEM-X InSAR data and high-density ALS for the prediction of forest inventory attributes in plantation forests with steep terrain. *Remote Sensing of Environment* 246, 111833. URL: <https://www.sciencedirect.com/science/article/pii/S0034425720302030>, doi:10.1016/j.rse.2020.111833.
- Liu, H., Shen, X., Cao, L., Yun, T., Zhang, Z., Fu, X., Chen, X., Liu, F., 2021. Deep learning in forest structural parameter estimation using airborne LiDAR data. *IEEE Journal of Selected Topics in Applied Earth Observations and Remote Sensing* 14, 1603–1618. URL: <https://ieeexplore.ieee.org/document/9300163/>, doi:10.1109/JSTARS.2020.3046053.
- Luo, B., Yang, J., Shi, S., Gan, R., Wu, Z., Wang, S., Wang, A., Du, L., Gong, W., 2026. InceptionFormer: A deep learning framework for UAV LiDAR point cloud completion to improve tree parameters estimation in dense forests. *Remote Sensing of Environment* 338, 115348. URL: <https://www.sciencedirect.com/science/article/pii/S0034425726000000>.

//linkinghub.elsevier.com/retrieve/pii/S0034425726001185,
doi:10.1016/j.rse.2026.115348.

- Maltamo, M., Packalen, P., Laukkanen, L., Korhonen, L., 2025. The transferability and cross-use of airborne laser scanning-based leaf-off and leaf-on biomass models. *European Journal of Remote Sensing* 58, 2542870. URL: <https://doi.org/10.1080/22797254.2025.2542870>, doi:10.1080/22797254.2025.2542870. publisher: Taylor & Francis _eprint: <https://doi.org/10.1080/22797254.2025.2542870>.
- Matasci, G., Hermosilla, T., Wulder, M.A., White, J.C., Coops, N.C., Hobart, G.W., Zald, H.S.J., 2018. Large-area mapping of Canadian boreal forest cover, height, biomass and other structural attributes using Landsat composites and lidar plots. *Remote Sensing of Environment* 209, 90–106. URL: <https://www.sciencedirect.com/science/article/pii/S0034425717305953>, doi:10.1016/j.rse.2017.12.020.
- Miettinen, J., Breidenbach, J., Adame, P., Adolt, R., Alberdi, I., Antropov, O., Arnarsson, O., Astrup, R., Berger, A., Bogason, J., Chirici, G., Corona, P., D'Amico, G., Fejfar, J., Fischer, C., Gohon, F., Gschwantner, T., Hertzer, J., Koma, Z., Korhonen, K.T., Krajnc, L., Latte, N., Lejeune, P., McCullagh, A., Mionskowski, M., Moreno-Fernández, D., Myllymäki, M., Nilsson, M., Perin, J., Pitkänen, J., Redmond, J., Riedel, T., Schumacher, J., Seitsonen, L., Sirro, L., Skudnik, M., Snorrason, A., Sroga, R., Traub, B., Traustason, B., Westerlund, B., Wurpillot, S., 2025. Pan-European forest maps produced with a combination of earth observation data and national forest inventory plots. *Data in Brief* 60, 111613. URL: <https://www.sciencedirect.com/science/article/pii/S2352340925003452>, doi:10.1016/j.dib.2025.111613.
- Moran, C.J., Kane, V.R., Seielstad, C.A., 2020. Mapping forest canopy fuels in the western United States with LiDAR–Landsat covariance. *Remote Sensing* 12. URL: <https://www.mdpi.com/2072-4292/12/6/1000>, doi:10.3390/rs12061000. publisher: Multidisciplinary Digital Publishing Institute.
- Moudrý, V., Gdulová, K., Fogl, M., Klápště, P., Urban, R., Komárek, J., Moudrá, L., Štroner, M., Barták, V., Solský, M., 2019. Comparison of leaf-off and leaf-on combined UAV imagery and airborne LiDAR for assessment of a post-mining site terrain and vegetation structure: Prospects

- for monitoring hazards and restoration success. *Applied Geography* 104, 32–41. URL: <https://www.sciencedirect.com/science/article/pii/S0143622818305897>, doi:10.1016/j.apgeog.2019.02.002.
- Narine, L.L., Popescu, S.C., Malambo, L., 2023. A methodological framework for mapping canopy cover using ICESat-2 in the southern USA. *Remote Sensing* 15. URL: <https://www.mdpi.com/2072-4292/15/6/1548>, doi:10.3390/rs15061548. publisher: Multidisciplinary Digital Publishing Institute.
- Nilsson, M., Nordkvist, K., Jonzén, J., Lindgren, N., Axensten, P., Wallerman, J., Egberth, M., Larsson, S., Nilsson, L., Eriksson, J., Olsson, H., 2017. A nationwide forest attribute map of Sweden predicted using airborne laser scanning data and field data from the National Forest Inventory. *Remote Sensing of Environment* 194, 447–454. URL: <https://www.sciencedirect.com/science/article/pii/S0034425716303947>, doi:10.1016/j.rse.2016.10.022.
- Næsset, E., 2009. Effects of different sensors, flying altitudes, and pulse repetition frequencies on forest canopy metrics and biophysical stand properties derived from small-footprint airborne laser data. *Remote Sensing of Environment* 113, 148–159. URL: <https://www.sciencedirect.com/science/article/pii/S0034425708002691>, doi:10.1016/j.rse.2008.09.001.
- Oehmcke, S., Li, L., Trepekli, K., Revenga, J., Nord-Larsen, T., Gieseke, F., Igel, C., 2023. Deep learning based 3D point cloud regression for estimating forest biomass. URL: <http://arxiv.org/abs/2112.11335>, doi:10.48550/arXiv.2112.11335. arXiv:2112.11335 [cs].
- Oehmcke, S., Li, L., Trepekli, K., Revenga, J.C., Nord-Larsen, T., Gieseke, F., Igel, C., 2024. Deep point cloud regression for above-ground forest biomass estimation from airborne LiDAR. *Remote Sensing of Environment* 302, 113968. URL: <https://linkinghub.elsevier.com/retrieve/pii/S0034425723005205>, doi:10.1016/j.rse.2023.113968.
- Parra, L.A.R., Bindner, R., Cordonnier, T., Renaud, J.P., Hertzog, L., Besic, N., Bontemps, J.D., Vega, C., 2025. Fiabilité des modèles de télédétection établis sur de grands territoires forestiers : une analyse de leur applicabilité à l'échelle locale. *Revue forestière française* 76, 173–185. URL: <https://>

revueforestierefrancaise.agroparistech.fr/article/view/9611,
doi:10.20870/revforfr.2025.9611.

- Pearse, G.D., Dash, J.P., Persson, H.J., Watt, M.S., 2018. Comparison of high-density LiDAR and satellite photogrammetry for forest inventory. *ISPRS Journal of Photogrammetry and Remote Sensing* 142, 257–267. URL: <https://www.sciencedirect.com/science/article/pii/S0924271618301709>, doi:10.1016/j.isprsjprs.2018.06.006.
- Perez, E., Strub, F., Vries, H.d., Dumoulin, V., Courville, A., 2018. FiLM: Visual reasoning with a general conditioning layer, in: *AAAI*. doi:10.48550/arXiv.1709.07871. arXiv:1709.07871.
- Petras, V., Petrasova, A., McCarter, J.B., Mitasova, H., Meentemeyer, R.K., 2023. Point density variations in airborne Lidar point clouds. *Sensors* 23, 1593. URL: <https://www.mdpi.com/1424-8220/23/3/1593>, doi:10.3390/s23031593.
- Qin, H., Wang, C., Xi, X., Tian, J., Zhou, G., 2017. Simulating the effects of the airborne Lidar scanning angle, flying altitude, and pulse density for forest foliage profile retrieval. *Applied Sciences* 7. URL: <https://www.mdpi.com/2076-3417/7/7/712>, doi:10.3390/app7070712.
- Raiaan, M.A.K., Sakib, S., Fahad, N.M., Mamun, A.A., Rahman, M.A., Shatabda, S., Mukta, M.S.H., 2024. A systematic review of hyperparameter optimization techniques in Convolutional Neural Networks. *Decision Analytics Journal* 11, 100470. URL: <https://www.sciencedirect.com/science/article/pii/S2772662224000742>, doi:10.1016/j.dajour.2024.100470.
- Rodes-Blanco, M., Ruiz-Benito, P., Silva, C.A., García, M., 2023. Canopy gap patterns in Mediterranean forests: a spatio-temporal characterization using airborne LiDAR data. *Landscape Ecology* 38, 3427–3442. URL: <https://doi.org/10.1007/s10980-023-01663-5>, doi:10.1007/s10980-023-01663-5.
- Roussel, J.R., Auty, D., Coops, N.C., Tompalski, P., Goodbody, T.R.H., Meador, A.S., Bourdon, J.F., de Boissieu, F., Achim, A., 2020. lidR: An R package for analysis of Airborne Laser Scanning (ALS) data. *Remote Sensing of Environment* 251, 112061. URL: <https://www.sciencedirec>

t.com/science/article/pii/S0034425720304314, doi:10.1016/j.rse.2020.112061.

- Rüetschi, M., Weber, D., Koch, T.L., Waser, L.T., Small, D., Ginzler, C., 2021. Countrywide mapping of shrub forest using multi-sensor data and bias correction techniques. *International Journal of Applied Earth Observation and Geoinformation* 105, 102613. URL: <https://linkinghub.elsevier.com/retrieve/pii/S0303243421003202>, doi:10.1016/j.jag.2021.102613.
- Saarela, S., Holm, S., Grafström, A., Schnell, S., Næsset, E., Gregoire, T.G., Nelson, R.F., Ståhl, G., 2016. Hierarchical model-based inference for forest inventory utilizing three sources of information. *Annals of Forest Science* 73, 895–910. URL: <https://doi.org/10.1007/s13595-016-0590-1>, doi:10.1007/s13595-016-0590-1.
- Sagar, A., Vega, C., Bouriaud, O., Piedallu, C., Renaud, J.P., 2025. Forest attribute maps: a support for small area estimation of forest disturbances. *Annals of Forest Science* 82, 23. URL: <https://doi.org/10.1186/s13595-025-01293-8>, doi:10.1186/s13595-025-01293-8.
- Seely, H., Coops, N.C., White, J.C., Montwé, D., Winiwarter, L., Ragab, A., 2023. Modelling tree biomass using direct and additive methods with point cloud deep learning in a temperate mixed forest. *Science of Remote Sensing* 8, 100110. URL: <https://linkinghub.elsevier.com/retrieve/pii/S2666017223000354>, doi:10.1016/j.srs.2023.100110.
- Simpson, J.E., Smith, T.E.L., Wooster, M.J., 2017. Assessment of errors caused by forest vegetation structure in Airborne LiDAR-derived DTMs. *Remote Sensing* 9. URL: <https://www.mdpi.com/2072-4292/9/11/1101>, doi:10.3390/rs9111101. publisher: Multidisciplinary Digital Publishing Institute.
- Soininen, V., Yu, X., Hyypä, M., Hyypä, J., 2025. Transferability of country-wide airborne laser scanning-based models for individual-tree attributes. *Science of Remote Sensing* 12, 100310. URL: <https://www.sciencedirect.com/science/article/pii/S2666017225001166>, doi:10.1016/j.srs.2025.100310.

- Tomppo, E., Olsson, H., Ståhl, G., Nilsson, M., Hagner, O., Katila, M., 2008. Combining national forest inventory field plots and remote sensing data for forest databases. *Remote Sensing of Environment* 112, 1982–1999. URL: <https://linkinghub.elsevier.com/retrieve/pii/S0034425708000242>, doi:10.1016/j.rse.2007.03.032.
- Vega, C., Hamrouni, A., El Mokhtari, S., Morel, J., Bock, J., Renaud, J.P., Bouvier, M., Durrieu, S., 2014. PTrees: A point-based approach to forest tree extraction from lidar data. *International Journal of Applied Earth Observation and Geoinformation* 33, 98–108. URL: <https://www.sciencedirect.com/science/article/pii/S0303243414001135>, doi:10.1016/j.jag.2014.05.001.
- Vidal, C., Alberdi, I., Hernández Mateo, L., Redmond, J., 2016. National forest inventories: Assessment of wood availability and use. doi:10.1007/978-3-319-44015-6. journal Abbreviation: National Forest Inventories: Assessment of Wood Availability and Use Pages: 845 Publication Title: National Forest Inventories: Assessment of Wood Availability and Use.
- Villikka, M., Packalén, P., Maltamo, M., 2012. The suitability of leaf-off airborne laser scanning data in an area-based forest inventory of coniferous and deciduous trees. *Silva Fennica* 46. URL: <https://www.silvafennica.fi/article/68>.
- Walshe, D., McInerney, D., Pereira, J.P., Byrne, K.A., 2021. Investigating the effects of k and area size on variance estimation of multiple pixel areas using a k-NN technique for forest parameters. *Remote Sensing* 13. URL: <https://www.mdpi.com/2072-4292/13/22/4688>, doi:10.3390/rs13224688. publisher: Multidisciplinary Digital Publishing Institute.
- Wang, P.S., Liu, Y., Guo, Y.X., Sun, C.Y., Tong, X., 2017. O-CNN: octree-based convolutional neural networks for 3D shape analysis. *ACM Transactions on Graphics* 36, 1–11. URL: <https://dl.acm.org/doi/10.1145/3072959.3073608>, doi:10.1145/3072959.3073608.
- Wasser, L., Day, R., Chasmer, L., Taylor, A., 2013. Influence of vegetation structure on Lidar-derived canopy height and fractional cover in forested riparian buffers during leaf-off and leaf-on conditions. *PLoS ONE* 8, e54776. URL: <https://www.ncbi.nlm.nih.gov/pmc/articles/PMC3561319/>, doi:10.1371/journal.pone.0054776.

- Wegen, O., Scheibel, W., Richter, R., Döllner, J., 2025. A survey of publicly available multi-temporal point cloud datasets. *ISPRS Journal of Photogrammetry and Remote Sensing* 231, 815–836. URL: <https://www.sciencedirect.com/science/article/pii/S0924271625004423>, doi:10.1016/j.isprsjprs.2025.11.003.
- White, J.C., Arnett, J.T., Wulder, M.A., Tompalski, P., Coops, N.C., 2015. Evaluating the impact of leaf-on and leaf-off airborne laser scanning data on the estimation of forest inventory attributes with the area-based approach. *Canadian Journal of Forest Research* 45, 1498–1513. URL: <https://cdnsiencepub.com/doi/10.1139/cjfr-2015-0192>, doi:10.1139/cjfr-2015-0192. publisher: NRC Research Press.
- Wu, X., Jiang, L., Wang, P.S., Liu, Z., Liu, X., Qiao, Y., Ouyang, W., He, T., Zhao, H., 2024. Point Transformer V3: Simpler, Faster, Stronger. URL: <http://arxiv.org/abs/2312.10035>, doi:10.48550/arXiv.2312.10035. arXiv:2312.10035 [cs].
- Ørka, H.O., Næsset, E., Bollandsås, O.M., 2010. Effects of different sensors and leaf-on and leaf-off canopy conditions on echo distributions and individual tree properties derived from airborne laser scanning. *Remote Sensing of Environment* 114, 1445–1461. URL: <https://www.sciencedirect.com/science/article/pii/S003442571000057X>, doi:10.1016/j.rse.2010.01.024.